# Low Intensity Vibration Restores Nuclear YAP Levels and Acute YAP Nuclear Shuttling in Mesenchymal Stem Cells Subjected to Simulated Microgravity

Thompson M[1], Woods K[2], Newberg, J[1], Oxford JT[2], Uzer G[1†]

[1] Mechanical and Biomedical Engineering, Boise State University

[2] Biomolecular Sciences Graduate Program, Boise State University

**[†] Corresponding Author**

**Running title:** LIV rescues SMG-inhibited YAP nuclear entry

Funding support: NASA ISGC NNX15AI04H, NIH R01AG059923, and 5P2CHD086843-03, P20GM109095, P20GM103408 and NSF 1929188.

**[†] Corresponding author:**

Gunes Uzer PhD

Boise State University

Department of Mechanical and Biomedical Engineering

1910 University Drive, MSd-2085

Boise, ID 83725-2085

Ph. (208) 426-4461

**Email: gunesuzer@boisestate.edu**

**Abstract**

Reducing the bone deterioration that astronauts experience in microgravity requires countermeasures that can improve the effectiveness of rigorous and time-expensive exercise regimens under microgravity. The ability of low intensity vibrations (LIV) to activate force-responsive signaling pathways in cells suggests LIV as a potential countermeasure to improve cell responsiveness to subsequent mechanical challenge. Mechanoresponse of mesenchymal stem cells (MSC) which maintain bone-making osteoblasts is in part controlled by the "mechanotransducer" protein YAP (Yes-associated protein) which is shuttled into the nucleus in response cyto-mechanical forces. Here, using YAP nuclear shuttling as a measure of MSC mechanoresponse, we tested the effect of 72 hours of simulated microgravity (SMG) and daily LIV application ($LIV_{DT}$) on the YAP nuclear entry driven by either acute LIV ($LIV_{AT}$) or Lysophosphohaditic acid (LPA), applied at the end of the 72h period. We hypothesized that SMG-induced impairment of acute YAP nuclear entry will be alleviated by daily application of $LIV_{DT}$. Results showed that while both acute $LIV_{AT}$ and LPA treatments increased nuclear YAP entry by 50% and 87% over the basal levels in SMG-treated MSCs, nuclear YAP levels of all SMG groups were significantly lower than non-SMG controls. Daily dosing of $LIV_{DT}$, applied in parallel to SMG, restored the SMG-driven decrease in basal nuclear YAP to control levels as well as increased the LPA-induced but not $LIV_{AT}$-induced YAP nuclear entry over the non-$LIV_{DT}$ treated, SMG only, counterparts. These cell level observations suggest that utilizing daily LIV treatments is a feasible countermeasure for increasing the YAP-mediated anabolic responsiveness of MSCs to subsequent mechanical challenge under SMG.

**Key Words:** Simulated Microgravity, Low Intensity Vibrations, YAP, Nucleus, Mesenchymal Stem Cells, Mechanosignaling

53 **Introduction**

54 The musculoskeletal deterioration which astronauts experience on long-term space missions
55 and the resulting increase of traumatic physical injury risk is in part due to the reduction of
56 mechanical loading on the musculoskeleton [1]. To alleviate the detrimental effects of unloading,
57 astronauts undergo intensive regimens of running and resistance training in orbit [2]. Despite
58 these efforts, astronauts lose an average bone density of 1% for each month they spend in
59 space [3]. This loss necessitates new non-pharmacologic therapies in addition to exercise to keep
60 bones healthy during long-term space missions. In bone, tissue level response to mechanical
61 challenge is in part regulated by osteoblasts and osteocytes [4]. Both osteoblasts and osteocytes
62 in turn share a common progenitor: the mesenchymal stem cell (MSC). Therefore, the growth
63 and differentiation of MCSs in response to mechanical stimulation is required for the
64 maintenance and repair of bone [5]. It is for this reason that the MSCs are a potential target for
65 mechanical therapies aiming to alleviate bone loss in astronauts, injured service personnel with
66 long periods of bedrest, and physically inactive aged individuals [6].

67

68 To maintain healthy bone making cell populations, MSCs rely on environmental mechanical
69 signals inside the bone marrow niches and near bone surfaces. While the exact characteristics
70 of the mechanical environment in which MSCs exist remains to be quantified, it is known that
71 during habitual activities, our bones are subjected to combinations of complex loads including
72 strain, fluid shear, and acceleration, each of which is inseparable [7]. For example, during
73 moderate running, cortical bone can experience strains up to 2000με [8,9], which also generates
74 coupled fluid flow within canaliculi of up to 100μm/s [10]. The interior of bone is filled with bone
75 marrow with viscosities in the range of 400-800cP [11]. During moderate running, tibial
76 accelerations are within the 2-5g range [12] (1g = 9.81 m/s$^2$), creating a complex loading at the
77 bone-marrow interface that depends on many factors including frequency, amplitude, and
78 viscosity [13]. *In silico* studies reveal that when exposed to vibrations (0.1-2g), marrow-filled

trabecular compartments generate fluid shear stresses up to 2Pa [13,14], capable of driving bone cell functions [15]. Interestingly, while these high magnitude forces are only experienced a few times during the day, bones are bombarded by smaller mechanical signals arising from muscle contractions that generate bone strains ranging between 2 to 10με [16]. Exogenous application of small magnitude mechanical regimes in the form of low intensity vibrations (LIV) ranging between 0.1-2g acceleration magnitudes and 20-200Hz frequencies were shown to be effective in improving bone and muscle indices in clinical and preclinical studies [17]. At the cellular level, our group has reported that application of LIV increases MSC contractility [18], activates RhoA signaling [19], and results in increased osteogenic differentiation and proliferation of MSCs [20].

One of the most actively investigated signaling pathways that regulate the MSC mechanoresponse is the Yes-associated protein (YAP) signaling pathway. YAP depletion in stem cells results in reduced proliferation and osteogenesis [21,22]. Similarly, depleting YAP from osteoblast progenitors decreases both bone quality and quantity in mice [23]. Functionally, in response to cytomechanical forces and substrate stiffness, YAP moves from the cytoplasm to the nucleus where it interacts with its co-transcriptional activators such as TEAD to regulate gene expression related to proliferation [24]. For example, application of substrate strain induces YAP nuclear entry and YAP transcriptional activity which is required to activate proliferation [25]. While it has been shown that YAP nuclear entry is triggered by soluble factors that increase F-actin contractility such as Lysophosphatidic acid (LPA) [26,27], large changes in substrate stiffness [22], or substrate stretch ranging from 3% to 15% [25,28], it is not known if low magnitude signals like LIV also trigger acute YAP nuclear entry.

Research aimed at studying the effects of microgravity at the cellular level often relies on simulated microgravity (SMG) devices designed to alter the gravitational conditions that cells experience by rotating on one or multiple axes at low speed [29-31]. SMG decreases MSC

105 proliferation [32] and cytoskeletal contractility [29,33,34]. In this way, application of physical or soluble
106 factors that induce cytoskeletal contractility are commonly used as countermeasures for SMG
107 [35,36]. SMG also alters nuclear structure. Research from our group has shown that SMG results in
108 reduced levels of integral nuclear proteins such as Lamin A/C and LINC (Linker of
109 Nucleoskeleton and Cytoskeleton) complex elements Sun-2 [37]. As mechanically induced
110 nuclear shuttling of YAP and its paralog TAZ have been associated with LINC complex function
111 [38], SMG also results in decreased nuclear levels of the YAP paralog protein TAZ [35].
112 Interestingly, twice daily application of LIV for 20 minutes during SMG recovers both MSC
113 proliferation and levels of nuclear envelope proteins Lamin A/C and Sun-2, suggesting LIV as a
114 potential countermeasure to improve YAP-mediated mechanosignaling in MSCs under SMG.
115
116 In this study, using YAP nuclear shuttling as a measure of MSC mechanoresponse, we tested
117 the effect of 72 hours of simulated microgravity (SMG) and daily LIV application ($LIV_{DT}$) on the
118 YAP nuclear entry driven by either acute LIV ($LIV_{AT}$) or Lysophosphohaditic acid (LPA), applied
119 at the end of the 72h period. We hypothesized that SMG-induced impairment of YAP nuclear
120 entry in response to mechanical and soluble factors would be alleviated by daily application of
121 LIV.
122
123 **Results**
124 *Acute $LIV_{AT}$ application increases nuclear YAP levels*
125 To quantify the acute YAP nuclear entry in response to LIV, MSCs were plated at density of
126 5,200 cells/cm$^2$ and were allowed to attach for 24hr. Following this, MSCs were subjected to
127 treatment in two groups: control and acute LIV treatment regimen ($LIV_{AT}$). The $LIV_{AT}$ regimen
128 consisted of 5x 20min vibration periods separated by 1hr in between each repetition at room
129 temperature while control samples were treated identically (also taken out of the incubator) but
130 were not vibrated. Immediately after $LIV_{AT}$, samples were immunostained for YAP and DAPI.

131 MATLAB was used to quantify the changes in the nuclear YAP levels. As shown in **Fig.1a**,
132 confocal images showed increased nuclear YAP following the $LIV_{AT}$ treatment. Analysis of
133 confocal images to quantify nuclear YAP intensity shown in **Fig.1b** revealed a 32% increase in
134 the nuclear YAP levels in the $LIV_{AT}$ samples as compared to the control samples ($p<0.0001$).
135 We also used C2C12 myoblasts to confirm the $LIV_{AT}$ induced YAP nuclear entry on a second
136 cell line, quantitative analysis of confocal images showed a 40% increase of nuclear YAP in
137 $LIV_{AT}$ samples compared to controls (**Fig.S1**). As both LIV-induced focal adhesion signaling,
138 initiated by focal adhesion kinase (FAK) phosphorylation at Tyr 397 residue [19], and YAP nuclear
139 entry in response to substrate strain [28] requires intact LINC function, disabling LINC function via
140 a dominant negative overexpression of Nesprin KASH (Klarsicht, ANC-1, Syne homology)
141 fragment both decreased basal nuclear YAP levels by 34% ($p<0.0001$) and impeded the LIV-
142 induced YAP nuclear entry when compared to empty plasmid (**Fig.S2**). FAK phosphorylation at
143 Tyr 397 residue (pFAK) was blocked via a FAK inhibitor (FAKi) PF573228 (3μM) 1hr prior to
144 $LIV_{AT}$ treatment as previously described [19] and stained against DAPI and YAP (**Fig.S3a**). FAKi
145 inhibited the $LIV_{AT}$ induced pFAK and decreased its basal levels (**Fig.S3b**). As shown in
146 **Fig.S3c**, measuring nuclear YAP levels showed that $LIV_{AT}$ induced YAP nuclear entry was not
147 affected by FAKi when compared DMSO treated controls.
148
149 *Basal nuclear YAP levels decreased by SMG were rescued by daily application of $LIV_{DT}$*
150 We next tested whether SMG decreases basal YAP levels and whether a daily LIV treatment
151 regimen ($LIV_{DT}$), applied in parallel with SMG, could alleviate decreased YAP in the nucleus. As
152 we reported previously, $LIV_{DT}$ consisting of 2x 20min vibrations applied every 24 hours during
153 the 72h period of SMG. This $LIV_{DT}$ regimen was effective at restoring MSC proliferation and
154 whole cell YAP levels when applied in conjunction with SMG [37]. MSCs were plated at a density
155 of 1,700 cells/$cm^2$ in 9$cm^2$ tissue culture SlideFlasks (Nunc, #170920) and were allowed to
156 attach for 24h, after which point, the flasks were filled completely with growth medium, sealed,

157 and subjected to 72h of treatment followed by immunostaining for YAP and nuclear staining
158 using DAPI. During the 72h treatment period, MSCs were divided into three groups: control
159 samples, SMG samples which were subjected to the 72h SMG alone, and SMG+$LIV_{DT}$ samples
160 which were subjected to both the 72h SMG regimen and the daily $LIV_{DT}$ regimen.
161 Representative images for YAP and DAPI stained images are shown in **Fig.2a.** As depicted in
162 **Fig.2b**, quantitative analysis of confocal images revealed a 42% decrease in the nuclear YAP
163 intensity of the SMG group as compared to non-SMG controls ($p<0.0001$). Compared to the
164 SMG group, the $LIV_{DT}$ group increased nuclear YAP levels by 67% ($p<0.0001$) and there was no
165 significant difference between nuclear YAP levels of $LIV_{DT}$ treated MSCs and non-SMG controls.
166
167 *$LIV_{AT}$-induced YAP nuclear entry decreased by SMG was not restored by daily $LIV_{DT}$ application*
168 As SMG decreased basal nuclear YAP levels, we next tested whether SMG decreases $LIV_{AT}$-
169 induced YAP mechanosignaling (i.e. nuclear shuttling). Since $LIV_{DT}$ was able to restore nuclear
170 YAP levels (**Fig.2**), the SMG+$LIV_{DT}$ group was added to evaluate the effect of $LIV_{DT}$ on the SMG
171 response. A schematic of the experimental design is given in **Fig.3**. MSCs were divided into six
172 groups in which the CTRL, SMG, SMG+$LIV_{DT}$ groups were treated with ±$LIV_{AT}$ at the end of 72h
173 and nuclear YAP levels were measured. As shown in **Fig.4**, SMG alone decreased basal
174 nuclear YAP levels by 37% ($p<0.0001$) which were restored back to control levels in the
175 SMG+$LIV_{DT}$ group. As depicted in **Fig.4**, +$LIV_{AT}$ increased nuclear YAP levels in the CTRL,
176 SMG and SMG+$LIV_{DT}$ groups by 50%, 69% and 22%, respectively ($p<0.0001$) while exhibiting
177 the smallest increase in the SMG+$LIV_{DT}$. As a result, final nuclear YAP levels in the
178 SMG+$LIV_{DT}$+$LIV_{AT}$ group was not significantly different from the SMG+$LIV_{AT}$ and 23% lower than
179 the $LIV_{AT}$ group ($p<0.0001$). Representative confocal images are presented in **Fig.S4**.
180
181 *LPA treatment increases nuclear YAP levels*

182 As SMG+$LIV_{DT}$ treatment did not improve the acute $LIV_{AT}$ response when compared to the SMG
183 group, we next considered a soluble regulator of cytoskeletal contractility, LPA [20]. To test the
184 effect of LPA on the acute YAP nuclear entry, two LPA concentrations (50μM and 100μM) were
185 compared against control samples. Shown in **Fig.5**, nuclear YAP levels were almost doubled
186 under a two-hour exposure to 50μM LPA and 100μM LPA treatments with 99% and 107%
187 increases as compared to the control samples ($p<0.0001$). Nuclear YAP levels for 50μM LPA
188 and 100μM LPA treatments were not significantly different. Therefore, we chose to use 50μM
189 LPA treatment in the subsequent experiments.
190
191 *LPA-induced YAP nuclear entry decreased by SMG was alleviated by daily $LIV_{DT}$ application*
192 In order to evaluate whether $LIV_{DT}$ can restore LPA-induced YAP nuclear entry after SMG,
193 50μM LPA dissolved in DMSO or DMSO as vehicle control were added to the samples at the
194 end of the 72h treatment of either CTRL, SMG or SMG+$LIV_{DT}$ treatments. The CTRL group,
195 SMG group, and SMG+$LIV_{DT}$ group were subjected to the same treatment as in the previous
196 experiments and displayed similar results. As depicted in **Fig.6**, +LPA increased nuclear YAP
197 levels in the CTRL, SMG and SMG+$LIV_{DT}$ groups by 105%, 67% and 43% respectively
198 ($p<0.0001$). While final YAP nuclear levels in SMG+$LIV_{DT}$+LPA remained 70% higher than
199 SMG+LPA group ($P<0.0001$), it remained 29% lower than the LPA group ($P<0.0001$).
200
201 *MSC stiffness and structure remain intact under SMG and SMG+$LIV_{DT}$ treatments*
202 As YAP mechanosignaling of SMG+$LIV_{DT}$ MSCs remained below control levels in response to
203 both $LIV_{AT}$ and LPA, we quantified the effects of SMG and SMG+$LIV_{DT}$ on the cell stiffness, F-
204 actin intensity, cell area and nuclear area. AFM testing was used to quantify the elastic modulus
205 of the nucleus by measuring load-displacement curves on top of the nucleus. AFM tests shown
206 in **Fig.7a** indicated a 21% and 27% stiffness decrease in the SMG or SMG+$LIV_{DT}$ groups but
207 differences were not significant. Quantified from confocal images (**Fig.7b**), mean F-actin

208 intensities for all the cells in each imaging field were quantified by dividing the mean F-actin
209 intensity to the number of nuclei in each imaging field. Shown in **Fig.7c**, SMG and SMG+LIVDT
210 treated MSCs revealed 36% and 30% decreases in the mean F-actin intensity per cell,
211 respectively but the differences were not statistically significant. We have further quantified
212 nuclear area as a measure of cyto-mechanical forces on the nucleus [39]. Shown in **Fig.7d**,
213 analysis of cross-sectional area of cell nuclei using DAPI stained images revealed no significant
214 effect on average nuclear size by either SMG or combined SMG+$LIV_{DT}$ treatment compared to
215 control levels.
216

217 **Discussion**

218 The mechanical forces that the bone and muscle cells are subjected to on Earth and in
219 microgravity are complex and remain incompletely understood. At the same time, it is clear that
220 these forces are required for healthy tissue growth and function. The complexity of these forces
221 makes it difficult to design experiments that comprehensively simulate *in vivo* conditions. While
222 the *in vitro* experiments utilizing SMG and LIV treatments used in this study are limited in this
223 way and do not entirely correlate with the physiological behavior of these cells *in vivo*, the
224 experiments presented here remain useful for testing cell behavior under well-defined
225 conditions.
226

227 In this study, we focused on YAP mechanosignaling of MSCs. The first experiments
228 demonstrated that repeated $LIV_{AT}$ application over six hours was capable of stimulating YAP
229 entry into the nucleus in both MSCs (**Fig.1**) and in C2C12 cell line (**Fig.S1**). These findings
230 suggest that similar to high magnitude substrate strains [25] smaller mechanical signals such as
231 LIV can be effective at increasing nuclear YAP levels. Further, in agreement with earlier reports
232 utilizing uniaxial strain [28], $LIV_{AT}$-induced increase in nuclear YAP levels also required functional
233 LINC complexes (**Fig.S2**). Integrin related FAK signaling have been shown to promote YAP

234 nuclear levels in the proliferative descendants of stem cells and that FAK inhibitor PF573228
235 decreased nuclear YAP in these cells [40]. Similarly, inhibiting integrin engagement via blocking
236 FAK phosphorylation in Tyr 397 residue via FAKi also mutes the increase of GTP-bound RhoA
237 levels in LIV treated MSCs [19]. While we confirmed the loss of phosphorylation in Tyr 397 at both
238 basal level and in response to $LIV_{AT}$ (**Fig.S3b**), FAKi treatment changed neither basal levels nor
239 the $LIV_{AT}$-induced increase in nuclear YAP (**Fig.S3c**), suggesting a FAK independent
240 mechanism. In these experiments, we did not compare $LIV_{AT}$ with strain because the application
241 of 5 to 15% stretch onto sealed culture flasks was not technically possible without significantly
242 altering experimental conditions. Instead, LPA addition served as the best option for applying a
243 simple mechanical stimulation in order to evaluate the YAP mechanotransduction. LPA is a
244 phospholipid derivative signaling molecule which is capable of causing the simulation of static
245 transient stretch of a cell by increasing the contractility of the cytoskeleton [20,41]. The first
246 experiments with LPA served to verify that the simulation of stretch via increased cytoskeleton
247 contractility was capable of triggering YAP entry into the nucleus and the analysis methods
248 utilized here were capable of detecting this response (**Fig.5**).
249
250 The first SMG experiments confirmed a clear decrease of basal nuclear YAP levels.
251 Interestingly, SMG treated cells remained responsive, as both $LIV_{AT}$ and LPA treatments were
252 able to increase the nuclear YAP levels at the end of acute stimulation period (< 6h). However,
253 final nuclear YAP levels in SMG treated MSCs remained significantly lower when compared to
254 non-SMG groups (**Fig.2, 4 & 6**). These findings suggested that the YAP mechanosignaling
255 apparatus of MSCs, to some extent, was intact under SMG. When applied in parallel to SMG,
256 daily $LIV_{DT}$ treatment was able to restore basal YAP levels in the cell nucleus (**Fig.2, 4 & 6**)
257 measured 24h after the final $LIV_{DT}$ treatment. This increase in nuclear levels supported our
258 earlier report that showed sustained recovery of MSC proliferation by $LIV_{DT}$ [37].
259

260 Interestingly, this increase in basal nuclear YAP levels under $LIV_{DT}$ was accompanied by a
261 reduced MSC response to $LIV_{AT}$ treatment (**Fig.4**). When SMG+$LIV_{DT}$ treated MSCs were
262 subjected to $LIV_{AT}$, the increase in nuclear YAP from the non-$LIV_{AT}$ control was only 22%
263 ($p<0.0001$), which was small compared to the 77% increase seen in the SMG groups in
264 response to $LIV_{AT}$. As a result of this smaller increase in the SMG+$LIV_{DT}$ group, there was no
265 measurable difference between SMG and SMG+$LIV_{DT}$, samples that were subjected to $LIV_{AT}$. It
266 has been previously reported that an application of multiple LIV bouts separated by a refractory
267 period is more effective at activating mechano-signaling pathways such as βcatenin [42]. It is
268 possible that long term application of $LIV_{DT}$ results in cell structural adaptations that serve to
269 reduce MSC responsiveness to $LIV_{AT}$ treatment. To test this possibility, we replaced $LIV_{AT}$ with
270 an LPA treatment. When $LIV_{AT}$ was replaced by LPA treatment (**Fig.6**), responsiveness of
271 SMG+$LIV_{DT}$ treated MSCs almost doubled to 43% (compared to 22% in response to $LIV_{AT}$) and
272 was significantly higher than the SMG+LPA group ($p<0.0001$), suggesting that $LIV_{DT}$ increases
273 the YAP-mechanosignaling in response to LPA.
274
275 Absolute nuclear YAP intensity in the SMG+$LIV_{DT}$+$LIV_{AT}$ group, however, remained below the
276 $LIV_{AT}$ group ($p<0.0001$). Previously published findings using the same treatment protocols
277 suggested that the total cellular YAP levels decreased by SMG were restored to control levels
278 by daily LIV [37]. This indicates that total availability of YAP protein was not responsible for this
279 difference between the SMG+$LIV_{DT}$+$LIV_{AT}$ and the $LIV_{AT}$ groups. In regards to other potential
280 effects of SMG on the components of the mechanosignaling mechanism, one current prevailing
281 hypothesis suggests a role for nuclear pore opening in response to cyto-mechanical forces [38]
282 which may be affected by changes in the nuclear stiffness. To test this possibility, we performed
283 additional AFM and imaging experiments. While the AFM measured nuclear stiffness was 24%
284 lower in the SMG and SMG+$LIV_{DT}$ groups on average, we were unable to identify any
285 statistically significant effects of SMG or $LIV_{DT}$ treatment on nuclear stiffness. There was also

286 slight F-actin intensity decreases in both the SMG and SMG+$LIV_{DT}$ groups which were also not
287 significant (**Fig.7**). Similarly, cell and nuclear area were not affected. While our results were not
288 able to detect any changes in nuclear stiffness, considering the significant role that the nuclear
289 membrane plays as a mechanical structural component in the cell's interpretation of mechanical
290 stimulus [43,44], more detailed future studies are needed to study the effects of SMG on the
291 nuclear envelope and nuclear structure.
292
293 In summary, while the restoration of basal nuclear levels and improvement of LPA induced YAP
294 nuclear entry under daily $LIV_{DT}$ treatment identify LIV as a possible countermeasure to improve
295 MSC response under the detrimental effects of simulated microgravity, future studies are
296 required to understand why acute YAP nuclear entry in response to mechanical and soluble
297 factors remain less responsive.
298
299 **Methods and Materials**
300 *Cell Culture*
301 Primary mouse bone marrow derived MSC's were extracted as previously described [37,45].
302 C2C12 mouse myoblasts were derived from muscle satellite cells. MSCs were subcultured and
303 plated in Iscove modified Dulbecco's cell culture medium (IMDM, 12440053, Gibco) with 10%
304 fetal calf serum (FCS, S11950H, Atlanta Biologicals) and 1% pen/strep. C2C12s were
305 subcultured and plated in Dulbecco's modified Eagle's medium (DMEM, DML09, Caisson
306 Laboratories) with 10% fetal calf serum (FCS, S11950H, Atlanta Biologicals) and 1% pen/strep.
307 MSCs were subcultured in 9cm$^2$ culture dishes at a density of 5,200cells/cm$^2$ for 1day
308 experiments and 1700cells/cm$^2$ for 3day experiments, while C2C12s were plated at a density of
309 10,000cells/cm$^2$. Experimental cells were plated and given 24h to attach to the mounting surface
310 prior to experiments. Cell passages for both MSCs and C2C12s used for experiments were
311 limited to P7-P15.

312

313 *Low Intensity Vibrations Treatment*

314 SlideFlasks with plated MSCs were filled completely with culture medium and placed in LIV
315 device designed and used in previous research (**Fig.3**) [37]. LIV device subjected cells to low
316 intensity 90 Hz lateral vibrations at 0.7g at room temperature. MSCs were vibrated for 20min
317 intervals separated over time. $LIV_{AT}$ regimen was applied after 72h treatment period and
318 consisted of 5x 20min LIV with an hour in between each. Daily $LIV_{DT}$ regimen consisted of 3x
319 treatments in parallel with SMG treatment each consisting of 2x 20min LIV with 2h in between.

320

321 *Simulated Microgravity Treatment*

322 SlideFlasks (Nunc, #170920) with plated MSCs were filled completely with culture medium
323 (**Fig.3**) and placed in a clinostat SMG device. The clinostat shown is a redesign of a custom-
324 made clinostat described in previous research [37] with a new flask holder casing capable of
325 holding SlideFlasks and is also autoclavable. The clinostat was used to subject the MSCs to
326 constant 15 RPM SMG for 72h.

327

328 *Immunofluorescence Staining and Image Analysis*

329 Immediately after mechanical treatment, MSCs plated in Slideflasks were removed from
330 treatment, and the SlideFlasks were disassembled in order to stain the MSCs on the slides
331 (**Fig.3**). The MSCs were fixed with 4% paraformaldehyde, then washed and permeabilized with
332 0.05% Triton X-100 in PBS, followed by immunostaining with YAP specific antibody (YAP
333 (D8H1X) Rabbit mAb, Cell Signaling Technologies) and Alexa Fluor red secondary antibodies
334 (Donkey anti-Rabbit IgG (H+L) Cross-Adsorbed Secondary Antibody, Alexa Fluor Plus 594 for
335 all experiments prior to usage of LPA. Subsequently, Donkey anti-Rabbit IgG (H+L) Cross-
336 Adsorbed Secondary Antibody, Alexa Fluor Plus 633 was used). Nuclear DNA was labeled via
337 DAPI (Vectashield Mounting Medium, Vector Laboratories). Stained samples were imaged with

338 a Leica TCS SP8 confocal microscope (40x, HC PL APO CS2 Oil Immersion) prior to usage of
339 LPA, after this Zeiss LSM 510 Meta Confocal Microscope (40x, HC PL APO CS2 Oil Immersion)
340 . Exported images were used to quantify relative YAP levels within each nuclei (nuclear regions
341 traced by DAPI stained nucleus) via custom-made MATLAB program (The MathWorks, Natick,
342 MA). DAPI images were analyzed using an edge-detection algorithm in order to determine the
343 nuclear area for each cell. The nuclear outline was then used as a mask to quantify the average
344 pixel intensity of the YAP stain within the nuclei of each individual cell. (n=50-100
345 nuclei/sample).
346
347 *Atomic Force Microscopy*
348 Bruker Dimension FastScan AFM was used for collection of the atomic force measurements.
349 Tipless MLCT-D probes with a 0.03 N/m spring constant were functionalized with 10 μm
350 diameter borosilicate glass beads for force collection. The AFM's optical microscope was used
351 to locate individual live MSCs plated on the SlideFlask slides with the flask section removed for
352 access to the cells. The nucleus of each cell was tested with at least 3 seconds of rest between
353 each test. In each test, three force-displacement curves were obtained (ramping rate: 2 μm/sec
354 over 2 μm total travel, 1 μm approach, 1 μm retract), which were analyzed using Nanoscope
355 software with the implementation of a best-fit curve to a Hertzian (spherical) model (optimized
356 such that R^2 value was greater than 0.95, or $p<0.05$) to obtain elastic moduli of nuclear
357 membrane of individual nuclei.
358
359 *Western Blotting*
360 Western blotting was performed as previously described.[23,26,27,64] 20μg of lysed cell protein from
361 each sample was run on a 10% polyacrylamide gels, transferred onto a polyvinylidene difluoride
362 (PVDF) membranes, blocked with 5%( w/v) milk for 1h. After washing, primary antibodies were
363 incubated overnight at 4˚C with. Protein bands were visualized via horseradish peroxidase-

364 conjugated secondary antibodies (1: 5,000, Cell Signaling) and ECL plus chemiluminescence kit
365 (Amersham Biosciences, Piscataway, NJ) and scanned using C-DiGit blot scanner (Licor,
366 Lincoln, NE). All blots derive from the same experiment and were processed in parallel.
367
368 *Statistical analysis*
369 All data analysis results were displayed graphically based on the mean value with standard
370 error bars. Differences between treatments were not assumed to follow a Gaussian distribution.
371 Therefore, group differences were identified via either non-parametric two-tailed Mann-Whitney
372 U-test (**Fig.1a**) or Kruskal-Wallis test followed by Tukey multiple comparison (**Fig.2b, 4, 5, 6, 7,**
373 **&S1, S2, S3**). P-values of less than 0.05 were considered significant.
374
375 *Data availability*
376 The datasets generated and/or analyzed during the current study are available from the
377 corresponding author on reasonable request.
378
379 *Ethics*
380 All methods were carried out in accordance with relevant guidelines and regulations of Boise
381 Institutional Animal Care and Use Committee and Institutional Biosafety Committee. All
382 procedures were approved by Boise State University Institutional Animal Care and Use
383 Committee, and Institutional Biosafety Committee.
384
385 *Acknowledgements*
386 This study was supported by NASA ISGC NNX15AI04H, NIH R01AG059923, and
387 5P2CHD086843-03, P20GM109095, P20GM103408 and NSF 1929188.
388
389 *Competing interests*

390 The author(s) declare no competing interests, financial or otherwise.

391

392 *Contributions*

393 **Thompson, M** experimental methods, data analysis/interpretation, manuscript writing, final
394 approval of manuscript.

395 **Woods, K** data analysis/interpretation, final approval of manuscript.

396 **Newberg, J** experimental methods, final approval of manuscript

397 **Oxford JT**, financial support, final approval of manuscript

398 **Uzer, G** concept/design, financial support, data analysis/interpretation, manuscript writing, final
399 approval of manuscript

400

401 *References*


402 1 Smith, S. M. *et al.* Calcium metabolism before, during, and after a 3-mo spaceflight:
403 kinetic and biochemical changes. *Am J Physiol* **277**, R1-10 (1999).

404 2 Greenleaf, J. E., Bulbulian, R., Bernauer, E. M., Haskell, W. L. & Moore, T. Exercise-
405 training protocols for astronauts in microgravity. *Journal of applied physiology*
406 *(Bethesda, Md. : 1985)* **67**, 2191-2204, doi:10.1152/jappl.1989.67.6.2191 (1989).

407 3 Vico, L. *et al.* Effects of long-term microgravity exposure on cancellous and cortical
408 weight-bearing bones of cosmonauts. *Lancet (London, England)* **355**, 1607-1611 (2000).

409 4 Thompson, W. R., Rubin, C. T. & Rubin, J. Mechanical regulation of signaling pathways
410 in bone. *Gene* **503**, 179-193, doi:10.1016/j.gene.2012.04.076 (2012).

411 5 Ozcivici, E. *et al.* Mechanical signals as anabolic agents in bone. *Nature reviews.*
412 *Rheumatology* **6**, 50-59, doi:10.1038/nrrheum.2009.239 (2010).

413 6 Rando, T. A. & Ambrosio, F. Regenerative Rehabilitation: Applied Biophysics Meets
414 Stem Cell Therapeutics. *Cell Stem Cell* **22**, 306-309, doi:10.1016/j.stem.2018.02.003
415 (2018).

7 Chan, M. E., Uzer, G. & Rubin, C. The Potential Benefits and Inherent Risks of Vibration as a Non-Drug Therapy for the Prevention and Treatment of Osteoporosis. *Current osteoporosis reports*, 1-9, doi:10.1007/s11914-012-0132-1 (2013).

8 Judex, S., Gross, T. S. & Zernicke, R. F. Strain Gradients Correlate with Sites of Exercise-Induced Bone-Forming Surfaces in the Adult Skeleton. *Journal of Bone and Mineral Research* **12**, 1737-1745, doi:10.1359/jbmr.1997.12.10.1737 (1997).

9 Rubin, C. T. & Lanyon, L. E. Dynamic strain similarity in vertebrates; an alternative to allometric limb bone scaling. *Journal of Theoretical Biology* **107**, 321-327, doi:10.1016/s0022-5193(84)80031-4 (1984).

10 Price, C., Zhou, X. Z., Li, W. & Wang, L. Y. Real-Time Measurement of Solute Transport Within the Lacunar-Canalicular System of Mechanically Loaded Bone: Direct Evidence for Load-Induced Fluid Flow. *Journal of Bone and Mineral Research* **26**, 277-285, doi:10.1002/jbmr.211 (2011).

11 Gurkan, U. A. & Akkus, O. The Mechanical Environment of Bone Marrow: A Review. *Annals of biomedical engineering* **36**, 1978-1991, doi:10.1007/s10439-008-9577-x (2008).

12 Vainionpaa, A. *et al.* Intensity of exercise is associated with bone density change in premenopausal women. *Osteoporosis international : a journal established as result of cooperation between the European Foundation for Osteoporosis and the National Osteoporosis Foundation of the USA* **17**, 455-463, doi:10.1007/s00198-005-0005-x (2006).

13 Dickerson, D. A., Sander, E. A. & Nauman, E. A. Modeling the mechanical consequences of vibratory loading in the vertebral body: microscale effects. *Biomechanics and Modeling in Mechanobiology* **7**, 191-202, doi:10.1007/s10237-007-0085-y (2008).

441 14 Coughlin, T. R. & Niebur, G. L. Fluid shear stress in trabecular bone marrow due to low-
442 magnitude high-frequency vibration. *Journal of biomechanics* **45**, 2222-2229,
443 doi:10.1016/j.jbiomech.2012.06.020 (2012).
444 15 Riddle, R. C. & Donahue, H. J. From Streaming Potentials to Shear Stress: 25 Years of
445 Bone Cell Mechanotransduction. *Journal of Orthopaedic Research* **27**, 143-149,
446 doi:10.1002/jor.20723 (2009).
447 16 Fritton, S. P., McLeod, K. J. & Rubin, C. T. Quantifying the strain history of bone: spatial
448 uniformity and self-similarity of low-magnitude strains. *Journal of biomechanics* **33**, 317-
449 325, doi:10.1016/s0021-9290(99)00210-9 (2000).
450 17 Pagnotti, G. M. *et al.* Combating osteoporosis and obesity with exercise: leveraging cell
451 mechanosensitivity. *Nature Reviews Endocrinology*, doi:10.1038/s41574-019-0170-1
452 (2019).
453 18 Pongkitwitoon, S., Uzer, G., Rubin, J. & Judex, S. Cytoskeletal Configuration Modulates
454 Mechanically Induced Changes in Mesenchymal Stem Cell Osteogenesis, Morphology,
455 and Stiffness. *Scientific reports* **6**, 34791, doi:10.1038/srep34791 (2016).
456 19 Uzer, G. *et al.* Cell Mechanosensitivity to Extremely Low-Magnitude Signals Is Enabled
457 by a LINCed Nucleus. *STEM CELLS* **33**, 2063-2076, doi:10.1002/stem.2004 (2015).
458 20 Uzer, G., Pongkitwitoon, S., Ete Chan, M. & Judex, S. Vibration induced osteogenic
459 commitment of mesenchymal stem cells is enhanced by cytoskeletal remodeling but not
460 fluid shear. *Journal of Biomechanics* **46**, 2296-2302, doi:10.1016/j.jbiomech.2013.06.008
461 (2013).
462 21 Pan, J. X. *et al.* YAP promotes osteogenesis and suppresses adipogenic differentiation
463 by regulating beta-catenin signaling. *Bone research* **6**, 18, doi:10.1038/s41413-018-
464 0018-7 (2018).

465 22 Dupont, S. *et al.* Role of YAP/TAZ in mechanotransduction. *Nature* **474**, 179-183,
466 doi:http://www.nature.com/nature/journal/v474/n7350/abs/10.1038-nature10137-
467 unlocked.html#supplementary-information (2011).
468 23 Kegelman, C. D. *et al.* Skeletal cell YAP and TAZ combinatorially promote bone
469 development. *FASEB journal : official publication of the Federation of American*
470 *Societies for Experimental Biology* **32**, 2706-2721, doi:10.1096/fj.201700872R (2018).
471 24 Zhao, B. *et al.* TEAD mediates YAP-dependent gene induction and growth control.
472 *Genes & development* **22**, 1962-1971, doi:10.1101/gad.1664408 (2008).
473 25 Benham-Pyle, B. W., Pruitt, B. L. & Nelson, W. J. Cell adhesion. Mechanical strain
474 induces E-cadherin-dependent Yap1 and beta-catenin activation to drive cell cycle entry.
475 *Science (New York, N.Y.)* **348**, 1024-1027, doi:10.1126/science.aaa4559 (2015).
476 26 Ho, L. T. Y., Skiba, N., Ullmer, C. & Rao, P. V. Lysophosphatidic Acid Induces ECM
477 Production via Activation of the Mechanosensitive YAP/TAZ Transcriptional Pathway in
478 Trabecular Meshwork Cells. *Investigative Ophthalmology & Visual Science* **59**, 1969-
479 1984, doi:10.1167/iovs.17-23702 (2018).
480 27 Cai, H. & Xu, Y. The role of LPA and YAP signaling in long-term migration of human
481 ovarian cancer cells. *Cell Communication and Signaling* **11**, 31, doi:10.1186/1478-811X-
482 11-31 (2013).
483 28 Driscoll, Tristan P., Cosgrove, Brian D., Heo, S.-J., Shurden, Zach E. & Mauck,
484 Robert L. Cytoskeletal to Nuclear Strain Transfer Regulates YAP Signaling in
485 Mesenchymal Stem Cells. *Biophysical journal* **108**, 2783-2793,
486 doi:10.1016/j.bpj.2015.05.010 (2015).
487 29 Janmaleki, M., Pachenari, M., Seyedpour, S. M., Shahghadami, R. & Sanati-Nezhad, A.
488 Impact of Simulated Microgravity on Cytoskeleton and Viscoelastic Properties of
489 Endothelial Cell. *Scientific reports* **6**, 32418, doi:10.1038/srep32418 (2016).

490 30 Qian, A. R. *et al.* Fractal Dimension as a Measure of Altered Actin Cytoskeleton in
491 MC3T3-E1 Cells Under Simulated Microgravity Using 3-D/2-D Clinostats. *Biomedical*
492 *Engineering, IEEE Transactions on* **59**, 1374-1380, doi:10.1109/TBME.2012.2187785
493 (2012).
494 31 Pardo, S. J. *et al.* Simulated microgravity using the Random Positioning Machine inhibits
495 differentiation and alters gene expression profiles of 2T3 preosteoblasts. *Am J Physiol*
496 *Cell Physiol* **288**, doi:10.1152/ajpcell.00222.2004 (2005).
497 32 Dai, Z. Q., Wang, R., Ling, S. K., Wan, Y. M. & Li, Y. H. Simulated microgravity inhibits
498 the proliferation and osteogenesis of rat bone marrow mesenchymal stem cells. *Cell*
499 *proliferation* **40**, 671-684, doi:10.1111/j.1365-2184.2007.00461.x (2007).
500 33 Shi, F. *et al.* Simulated Microgravity Promotes Angiogenesis through RhoA-Dependent
501 Rearrangement of the Actin Cytoskeleton. *Cellular physiology and biochemistry :*
502 *international journal of experimental cellular physiology, biochemistry, and pharmacology*
503 **41**, 227-238, doi:10.1159/000456060 (2017).
504 34 Corydon, T. J. *et al.* Reduced Expression of Cytoskeletal and Extracellular Matrix Genes
505 in Human Adult Retinal Pigment Epithelium Cells Exposed to Simulated Microgravity.
506 *Cellular physiology and biochemistry : international journal of experimental cellular*
507 *physiology, biochemistry, and pharmacology* **40**, 1-17, doi:10.1159/000452520 (2016).
508 35 Chen, Z., Luo, Q., Lin, C., Kuang, D. & Song, G. Simulated microgravity inhibits
509 osteogenic differentiation of mesenchymal stem cells via depolymerizing F-actin to
510 impede TAZ nuclear translocation. *Scientific reports* **6**, 30322, doi:10.1038/srep30322
511 (2016).
512 36 Uddin, S. M. & Qin, Y. X. Enhancement of osteogenic differentiation and proliferation in
513 human mesenchymal stem cells by a modified low intensity ultrasound stimulation under
514 simulated microgravity. *PLoS One* **8**, e73914, doi:10.1371/journal.pone.0073914 (2013).

515 37 Touchstone, H. *et al.* Recovery of stem cell proliferation by low intensity vibration under
516 simulated microgravity requires intact LINC complex *npj. Microgravity* **5**,
517 doi:doi.org/10.1038/s41526-019-0072-5 (2019).
518 38 Shiu, J.-Y., Aires, L., Lin, Z. & Vogel, V. Nanopillar force measurements reveal actin-
519 cap-mediated YAP mechanotransduction. *Nature cell biology* **20**, 262-271,
520 doi:10.1038/s41556-017-0030-y (2018).
521 39 Saeed, M. & Weihs, D. Finite element analysis reveals an important role for cell
522 morphology in response to mechanical compression. *Biomechanics and Modeling in*
523 *Mechanobiology*, doi:10.1007/s10237-019-01276-5 (2019).
524 40 Hu, J. K.-H. *et al.* An FAK-YAP-mTOR Signaling Axis Regulates Stem Cell-Based
525 Tissue Renewal in Mice. *Cell Stem Cell* **21**, 91-106.e106,
526 doi:10.1016/j.stem.2017.03.023 (2017).
527 41 Riddick, N., Ohtani, K. & Surks, H. K. Targeting by myosin phosphatase-RhoA
528 interacting protein mediates RhoA/ROCK regulation of myosin phosphatase. *Journal of*
529 *Cellular Biochemistry* **103**, 1158-1170, doi:10.1002/jcb.21488 (2008).
530 42 Sen, B. *et al.* Mechanical signal influence on mesenchymal stem cell fate is enhanced by
531 incorporation of refractory periods into the loading regimen. *Journal of biomechanics* **44**,
532 593-599, doi:10.1016/j.jbiomech.2010.11.022 (2011).
533 43 De Magistris, P. & Antonin, W. The Dynamic Nature of the Nuclear Envelope. *Current*
534 *biology : CB* **28**, R487-r497, doi:10.1016/j.cub.2018.01.073 (2018).
535 44 Czapiewski, R., Robson, M. I. & Schirmer, E. C. Anchoring a Leviathan: How the
536 Nuclear Membrane Tethers the Genome. *Frontiers in genetics* **7**, 82,
537 doi:10.3389/fgene.2016.00082 (2016).
538 45 Uzer, G. *et al.* Sun-mediated mechanical LINC between nucleus and cytoskeleton
539 regulates betacatenin nuclear access. *J Biomech* **74**, 32-40,
540 doi:10.1016/j.jbiomech.2018.04.013 (2018).

541

542 **Figure 1. Acute $LIV_{AT}$ application increases nuclear YAP levels.** (a) MSCs were subjected to
543 $LIV_{AT}$ and stained with DAPI (blue) and YAP (red). Confocal images indicated an increased
544 nuclear YAP levels following acute $LIV_{AT}$ applied as five 20min vibration periods separated by
545 1hr. (b) Quantitative analysis of confocal images showed a 32% of increase of nuclear YAP in
546 $LIV_{AT}$ samples compared to controls. n>400/grp, group comparison was made a Mann-Whitney
547 U-test, *p<0.05, **p<0.01, ***p<0.01, ****p<0.0001.

548

549 **Figure 2. Basal nuclear YAP levels decreased by SMG were rescued by $LIV_{DT}$.** (a) MSCs
550 were subjected to SMG, and SMG+$LIV_{DT}$ over 72h period and stained with DAPI (blue) and YAP
551 (red). (b) Quantitative analysis showed a 42% decrease of nuclear YAP levels in the SMG group
552 compared to control levels. The SMG+$LIV_{DT}$ group showed a 67% increase of nuclear YAP
553 when compared to the SMG group. There was no statistically significant difference between
554 CTRL and SMG+$LIV_{DT}$ groups. n>100/grp. Group comparisons were made via Kruskal-Wallis
555 test followed by Tukey multiple comparison, *p<0.05, **p<0.01, ***p<0.01, ****p<0.0001.

556

557 **Figure 3. Experimental design of combined SMG, $LIV_{AT}$ and $LIV_{DT}$ application.** MSCs were
558 subcultured and plated in SlideFlasks and allowed to attach for 24h before SlideFlasks were
559 filled with culture medium and sealed. Treatment regimen for MSC's involved 72h of SMG
560 (blue). $LIV_{DT}$ regimen consisted of one treatment cycle every 24hr during SMG treatment with
561 each cycle consisting of 2x 20min LIV with an hour in between (yellow). $LIV_{AT}$ regimen was
562 applied after 72h SMG treatment period and consisted of 5x 20min LIV with an hour in between
563 each (red). For LIV application, MSCs plated in SlideFlasks were placed in LIV device
564 constructed in the lab previous to this research. Vibrations were applied at peak magnitudes of
565 0.7 g at 90 Hz at room temperature. Control samples were treated the same but were not
566 vibrated. For SMG application, MSCs plated in SlideFlasks were secured in lab custom-built

567 clinostat inside incubator. The clinostat subjected the MSCs to constant 15 RPM rotation
568 simulated microgravity. After treatment, flasks were removed for immunofluorescence staining.
569
570 **Figure 4. $LIV_{AT}$-induced YAP nuclear entry decreased by SMG was not restored by daily**
571 **$LIV_{DT}$ application.** MSCs were subjected to either CTRL, SMG, SMG+$LIV_{DT}$ over 72h period
572 were subsequently treated with $LIV_{AT}$. Quantitative analysis of confocal images showed that
573 SMG alone decreased basal nuclear YAP levels by 37% which were increased back to control
574 levels in the SMG+$LIV_{DT}$ group. +$LIV_{AT}$ increased nuclear YAP levels in the CTRL, SMG and
575 SMG+$LIV_{DT}$ groups by 50%, 69% and 22%, respectively. Nuclear YAP intensity in the
576 SMG+$LIV_{DT}$+$LIV_{AT}$ group remained not significantly different from the SMG+$LIV_{AT}$ and 23%
577 smaller than the $LIV_{AT}$ group. n>200/grp. Group comparisons were made via Kruskal-Wallis test
578 followed by Tukey multiple comparison, *p<0.05, **p<0.01, ***p<0.01, ****p<0.0001.
579
580 **Figure 5. LPA treatment increases nuclear YAP levels.** (a) Representative confocal images
581 of DAPI (blue) and YAP (red) stained MSCs with or without LPA treatment. MSCs were
582 subjected to LPA addition at 50μM and 100μM concentrations. (b) Quantitative analysis of
583 confocal images revealed a 99% and a 107% increase in the 50μM LPA and 100μM LPA
584 treatments compared to DMSO treated controls, respectively. Nuclear YAP levels for 50μM LPA
585 and 100μM LPA treatments were not significantly different. n>30/grp. Group comparisons were
586 made via Kruskal-Wallis test followed by Tukey multiple comparison, *p<0.05, **p<0.01,
587 ***p<0.01, ****p<0.0001.
588
589 **Figure 6. LPA-induced YAP nuclear entry decreased by SMG was alleviated by daily $LIV_{DT}$**
590 **application.** MSCs were subjected to SMG, and parallel SMG+$LIV_{DT}$ over 72h period at the end
591 of 72h, samples were treated with either LPA (50μM) or DMSO. Quantitative analysis of
592 confocal images revealed that LPA addition increased nuclear YAP levels by 105%, 67% and

593 43% in the CTRL, SMG and SMG+$LIV_{DT}$ when compared to DMSO controls. When compared to
594 nuclear YAP intensity of the LPA treatment alone, SMG+LPA and SMG+$LIV_{DT}$+LPA samples
595 were 55% and 29% lower, respectively. YAP nuclear levels in SMG+$LIV_{DT}$+LPA remained 70%
596 higher than SMG+LPA group. n>100/grp. Group comparisons were made via Kruskal-Wallis test
597 followed by Tukey multiple comparison, *p<0.05, **p<0.01, ***p<0.01, ****p<0.0001.
598
599 **Figure 7. MSC stiffness and structure remain intact under SMG and SMG+$LIV_{DT}$**
600 **treatments.** MSCs were subjected to SMG and parallel SMG+$LIV_{DT}$ over a 72h period. (a)
601 Compared to CTRL samples, AFM measurement of the elastic moduli of SMG and SMG+$LIV_{DT}$
602 treated MSCs revealed apparent decreases in elastic modules that were 21% and 27% below
603 control levels, measured differences were not statistically significant. n=10/grp. (b)
604 Quantification of confocal images show that, (c) mean F-actin intensity of SMG and SMG+$LIV_{DT}$
605 treated MSCs revealed decrease of 36% and 30% below control levels, measured differences
606 were not statistically significant. n=15/grp. (d) No significant effects of either SMG or $LIV_{DT}$
607 treatment on the average nucleus size were found. n>100/grp. Group comparisons were made
608 via Kruskal-Wallis test followed by Tukey multiple comparison, *p<0.05, **p<0.01, ***p<0.01,
609 ****p<0.0001.
610
611 **Figure S1. $LIV_{AT}$ treatment increases nuclear YAP in C2C12 cells.** (a) C2C12 cells were
612 subjected to $LIV_{AT}$ and stained with DAPI (blue) and YAP (red). Confocal images displayed
613 increased nuclear YAP levels following $LIV_{AT}$ treatment. (b) Quantitative analysis of confocal
614 images showed a 40% increase of nuclear YAP in $LIV_{AT}$ samples compared to controls.
615 n>900/grp, group comparison was made using a Mann-Whitney U-test, *p<0.05, **p<0.01,
616 ***p<0.01, ****p<0.0001.
617

618 **Figure S2. LINC complex disruption decreases nuclear YAP levels and reduces $LIV_{AT}$-**
619 **induced YAP nuclear entry.** (a) Plasmids harboring either a dominant negative KASH domain
620 of Nesprin (DNK) to disable LINC complex function or empty mCherry control (MC) were
621 overexpressed in MSCs. Following puromycin selection, MC or DNK expressing MSCs were
622 subjected to $LIV_{AT}$ and stained against DAPI (blue) and YAP (red). (b) Quantitative analysis of
623 confocal images revealed a 49% increase of nuclear YAP following $LIV_{AT}$ in MC expressing
624 control MSCs. Basal YAP levels of the DNK-CTRL group were 34% lower compared to MC-
625 CTRL and $LIV_{AT}$ treatment failed to significantly increase nuclear YAP over DNK-CTRL (18%,
626 NS). n>30/grp, group comparisons were made via Kruskal-Wallis test followed by Tukey
627 multiple comparison, *p<0.05, **p<0.01, ***p<0.01, ****p<0.0001.
628
629 **Figure S3. Blocking FAK phosphorylation at Tyr 397 does not limit $LIV_{AT}$ induced YAP**
630 **nuclear entry.** Dimethyl sulphoxide (DMSO) or Tyr 397 specific FAK inhibitor (FAKi) PF573228
631 (3μM) was added to MSCs in culture medium for 1h prior to $LIV_{AT}$ or control treatments. (a)
632 Confocal images of YAP showed more intense nuclear YAP staining of $LIV_{AT}$ treated MSCs but
633 no apparent effect of FAKi when compared to DMSO (b) FAKi application 1hr prior to $LIV_{AT}$
634 treatment inhibited the $LIV_{AT}$ induced FAK phosphorylation at Tyr 397 and decreased the basal
635 levels (c) Quantitative analysis of confocal images revealed a 61% increase of nuclear YAP in
636 both the DMSO-LIV group and a 60% increase in the FAKi-$LIV_{AT}$ group compared to the DMSO-
637 CTRL group. Differences between the DMSO-CTRL and FAKi-CTRL groups and between the
638 DMSO-LIV and FAKi-$LIV_{AT}$ groups were not significant. n>50/grp. Group comparisons were
639 made via Kruskal-Wallis test followed by Tukey multiple comparison, *p<0.05, **p<0.01,
640 ***p<0.01, ****p<0.0001.
641
642 **Figure S4.** Confocal images for SMG/$LIV_{DT}$/$LIV_{AT}$ treatments in Figure 4.
643

644 **Figure S5.** Confocal images for SMG/LIV$_{DT}$/LPA treatment in Figure 6.

645

646 **Figure S6.** Unprocessed blots used in Figure S3 as obtained by LiCor C-DiGit blot scanner.

647

648 **Table S1:** Cell culture and pharmacological reagents and their final concentrations.

| Cell Culture and Pharmacological Reagents | | Final Concentration |
|---|---|---|
| IMDM | GIBCO | - |
| DMEM | Caisson Laboratories | - |
| FCS | Atlanta Biologicals | 10% v/v |
| Penicillin/streptomycin | GIBCO | 1% v/v |

649

650 **Table S2:** Antibodies used and their final concentrations for western blots.

| Antibodies | | Final Concentration |
|---|---|---|
| p-FAK Tyr397 (3283) | Cell Signaling | 1/1000 |
| FAK (sc-558) | Santa Cruz Biotechnology | 1/500 |
| LDHA (2012S) | Cell Signaling Technology | 1/1000 |

651

652 **Table S3:** Immunostaining antibodies and reagents and their final concentrations.

| Immunostaining antibodies and Reagents | | Final Concentration |
|---|---|---|
| DAPI (H-1500-10) | Vector Laboratories | 1 µg/mL |
| Alexa Fluor 488 Phalloidin | Life Technologies | 0.1µM |
| YAP (14074S) | Cell Signaling Technology | 1/100 |

653

**Figure 1.**

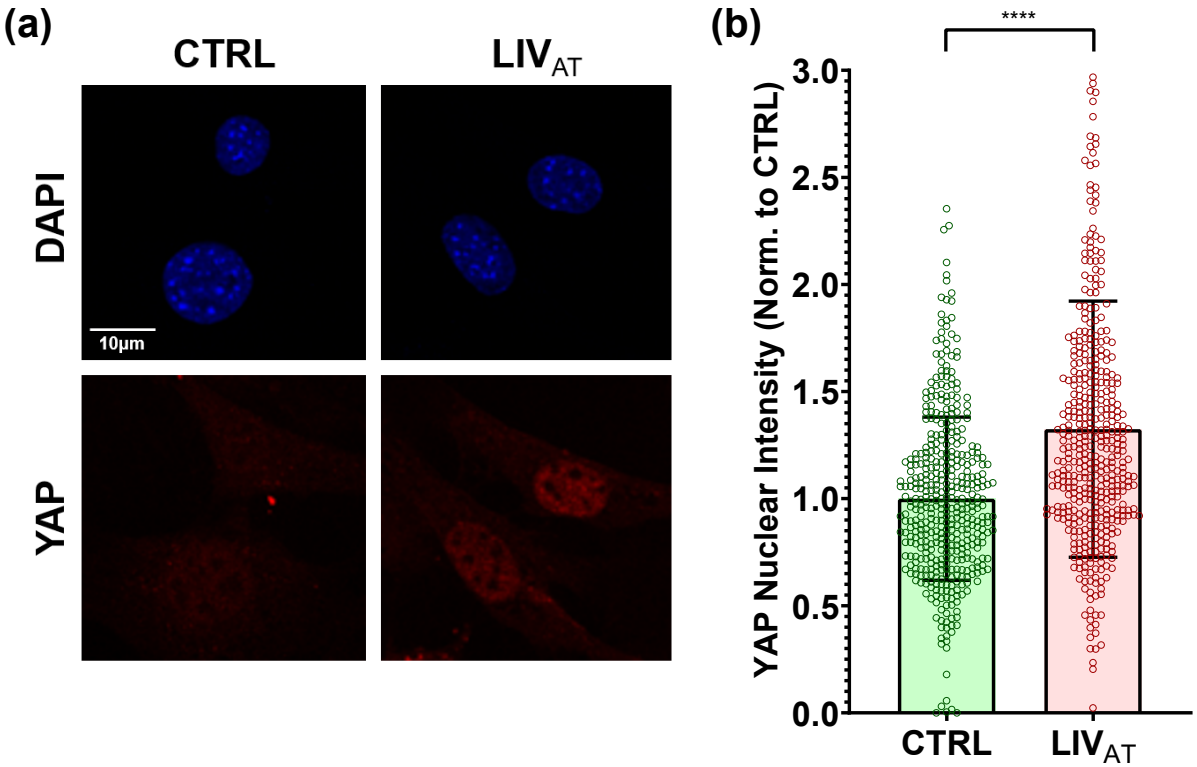


**Figure 1. Acute LIV$_{AT}$ application increases nuclear YAP levels.** (a) MSCs were subjected to LIV$_{AT}$ and stained with DAPI (blue) and YAP (red). Confocal images indicated an increased nuclear YAP levels following acute LIV$_{AT}$ applied as five 20min vibration periods separated by 1hr. (b) Quantitative analysis of confocal images showed a 32% of increase of nuclear YAP in LIV$_{AT}$ samples compared to controls. n>400/grp, group comparison was made a Mann-Whitney U-test, *p<0.05, **p<0.01, ***p<0.01, ****p<0.0001

**Figure 2.**

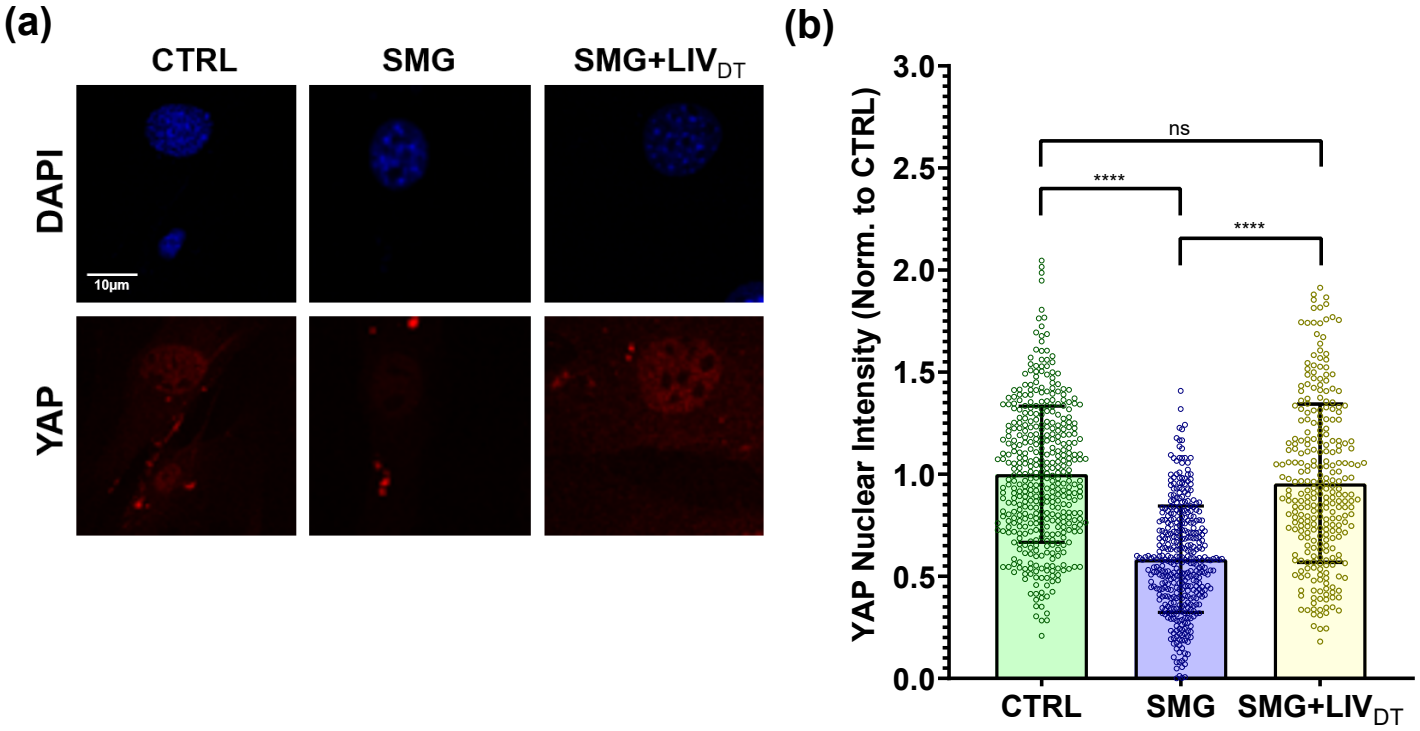


**Figure 2. Basal nuclear YAP levels decreased by SMG were rescued by LIV$_{DT}$.** (a) MSCs were subjected to SMG, and SMG+LIV$_{DT}$ over 72h period and stained with DAPI (blue) and YAP (red). (b) Quantitative analysis showed a 42% decrease of nuclear YAP levels in the SMG group compared to control levels. The SMG+LIV$_{DT}$ group showed a 67% increase of nuclear YAP when compared to the SMG group. There was no statistically significant difference between CTRL and SMG+LIV$_{DT}$ groups. n>100/grp. Group comparisons were made via Kruskal-Wallis test followed by Tukey multiple comparison, *p<0.05, **p<0.01, ***p<0.01, ****p<0.0001.

**Figure 3.**

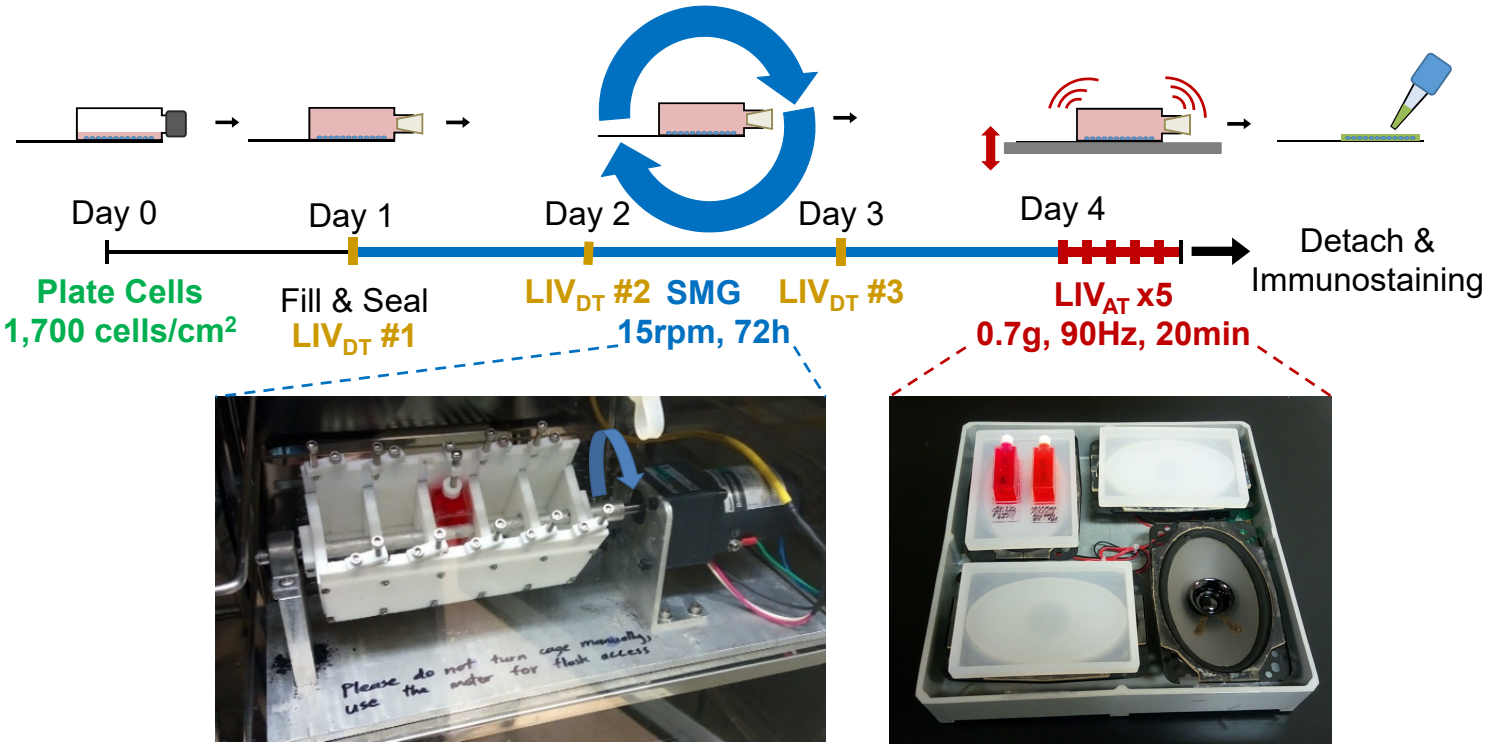


**Figure 3. Experimental design of combined SMG, LIV$_{AT}$ and LIV$_{DT}$ application.** MSCs were subcultured and plated in SlideFlasks and allowed to attach for 24h before SlideFlasks were filled with culture medium and sealed. Treatment regimen for MSC's involved 72h of SMG (blue). LIV$_{DT}$ regimen consisted of one treatment cycle every 24hr during SMG treatment with each cycle consisting of 2x 20min LIV with an hour in between (yellow). LIV$_{AT}$ regimen was applied after 72h SMG treatment period and consisted of 5x 20min LIV with an hour in between each (red). For LIV application, MSCs plated in SlideFlasks were placed in LIV device constructed in the lab previous to this research. Vibrations were applied at peak magnitudes of 0.7 g at 90 Hz at room temperature. Control samples were treated the same but were not vibrated. For SMG application, MSCs plated in SlideFlasks were secured in lab custom-built clinostat inside incubator. The clinostat subjected the MSCs to constant 15 RPM rotation simulated microgravity. After treatment, flasks were removed for immunofluorescence staining.

**Figure 4.**

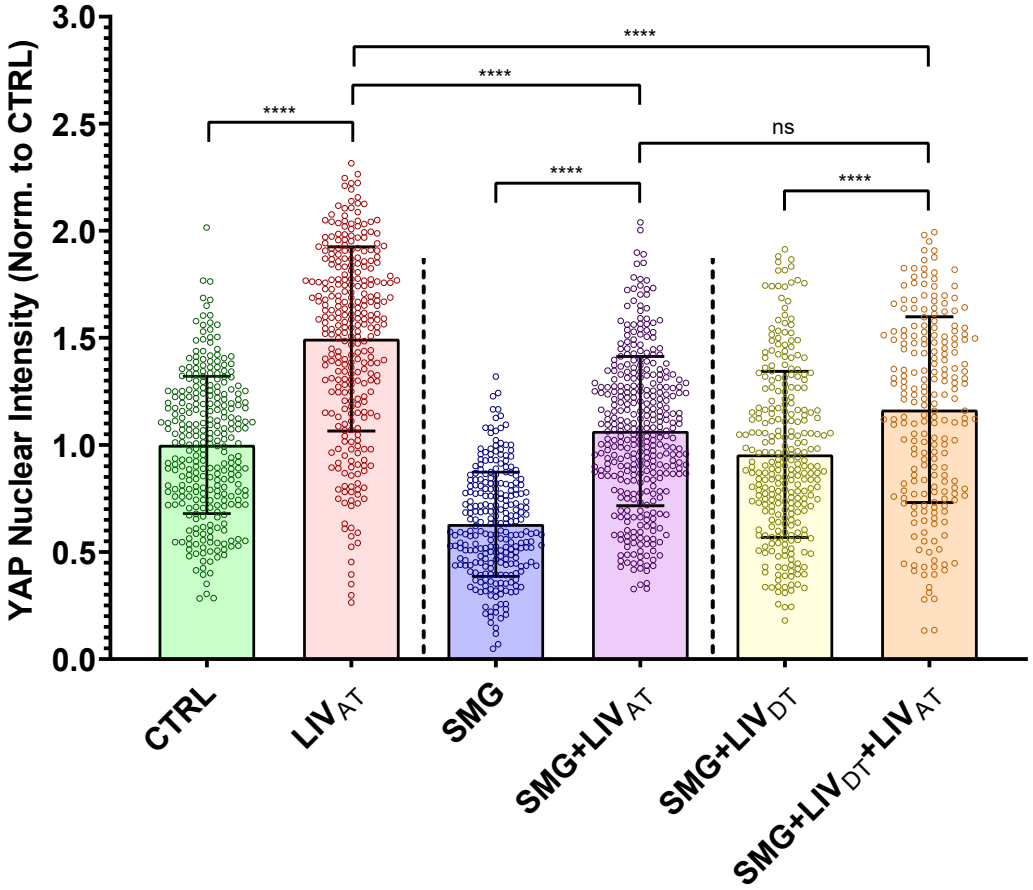


**Figure 4. LIV$_{AT}$-induced YAP nuclear entry decreased by SMG was not restored by daily LIV$_{DT}$ application.** MSCs were subjected to either CTRL, SMG, SMG+LIV$_{DT}$ over 72h period were subsequently treated with LIV$_{AT}$. Quantitative analysis of confocal images showed that SMG alone decreased basal nuclear YAP levels by 37% which were increased back to control levels in the SMG+LIV$_{DT}$ group. +LIV$_{AT}$ increased nuclear YAP levels in the CTRL, SMG and SMG+LIV$_{DT}$ groups by 50%, 69% and 22%, respectively. Nuclear YAP intensity in the SMG+LIV$_{DT}$+LIV$_{AT}$ group remained not significantly different from the SMG+LIV$_{AT}$ and 23% smaller than the LIV$_{AT}$ group. n>200/grp. Group comparisons were made via Kruskal-Wallis test followed by Tukey multiple comparison, *p<0.05, **p<0.01, ***p<0.01, ****p<0.0001.

**Figure 5.**

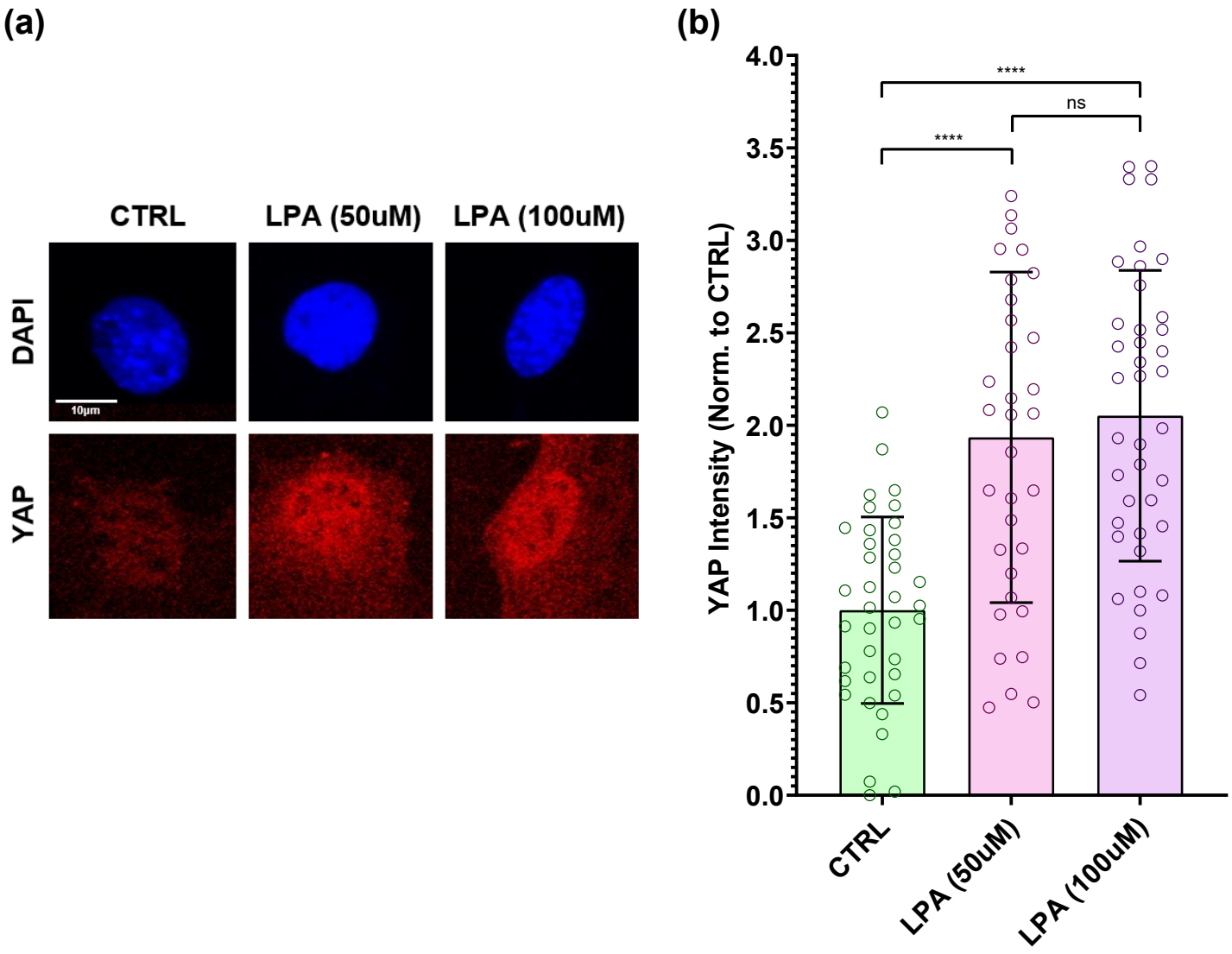


**Figure 5. LPA treatment increases nuclear YAP levels.** (a) Representative confocal images of DAPI (blue) and YAP (red) stained MSCs with or without LPA treatment. MSCs were subjected to LPA addition at 50µM and 100µM concentrations. (b) Quantitative analysis of confocal images revealed a 99% and a 107% increase in the 50µM LPA and 100µM LPA treatments compared to DMSO treated controls, respectively. Nuclear YAP levels for 50µM LPA and 100µM LPA treatments were not significantly different. n>30/grp. Group comparisons were made via Kruskal-Wallis test followed by Tukey multiple comparison, *$p<0.05$, **$p<0.01$, ***$p<0.01$, ****$p<0.0001$.

**Figure 6.**

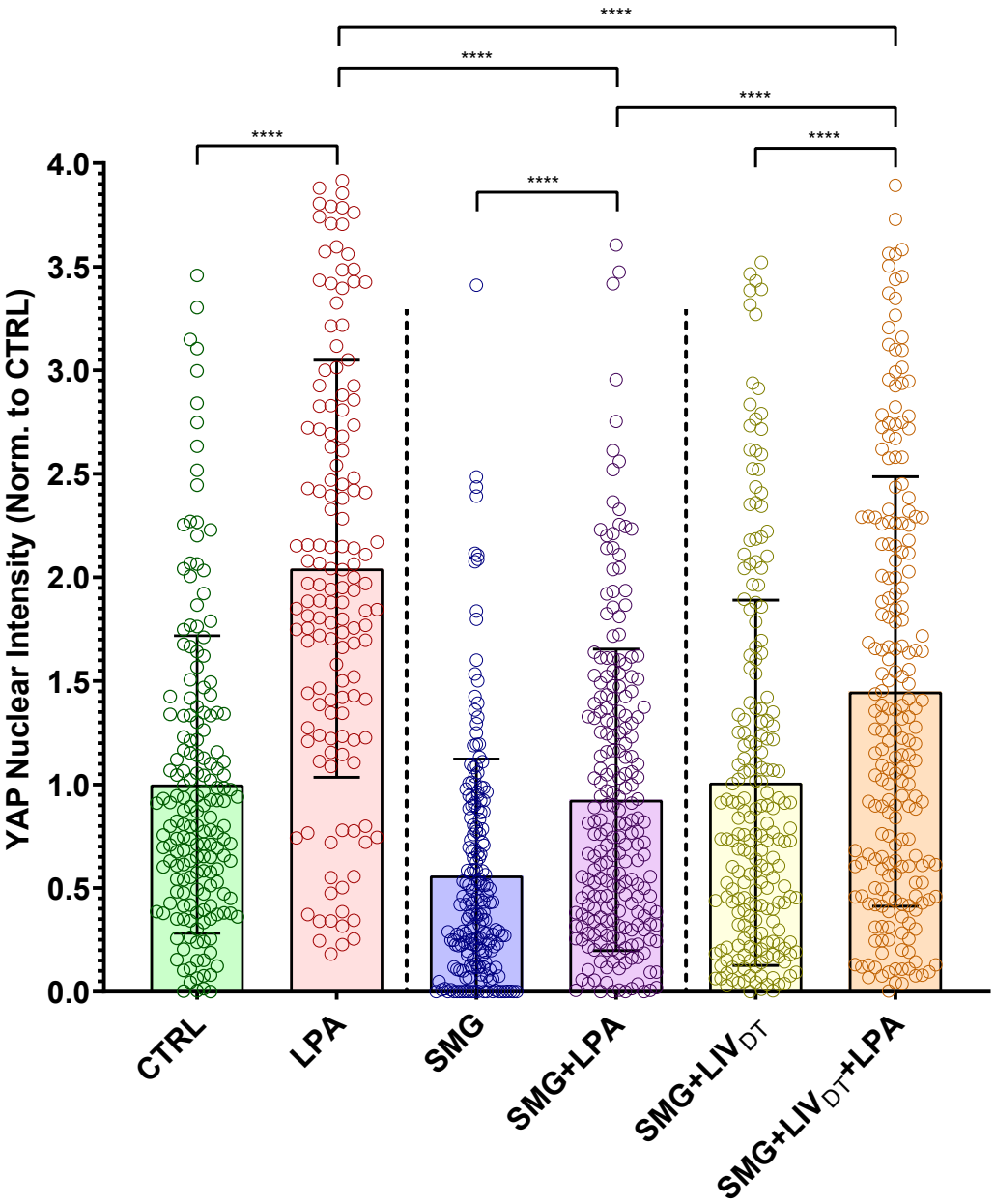


**Figure 6. LPA-induced YAP nuclear entry decreased by SMG was alleviated by daily LIV$_{DT}$ application.** MSCs were subjected to SMG, and parallel SMG+LIV$_{DT}$ over 72h period at the end of 72h, samples were treated with either LPA (50μM) or DMSO. Quantitative analysis of confocal images revealed that LPA addition increased nuclear YAP levels by 105%, 67% and 43% in the CTRL, SMG and SMG+LIV$_{DT}$ when compared to DMSO controls. When compared to nuclear YAP intensity of the LPA treatment alone, SMG+LPA and SMG+LIV$_{DT}$+LPA samples were 55% and 29% lower, respectively. YAP nuclear levels in SMG+LIV$_{DT}$+LPA remained 70% higher than SMG+LPA group. n>100/grp. Group comparisons were made via Kruskal-Wallis test followed by Tukey multiple comparison, *p<0.05, **p<0.01, ***p<0.01, ****p<0.0001.

**Figure 7.**

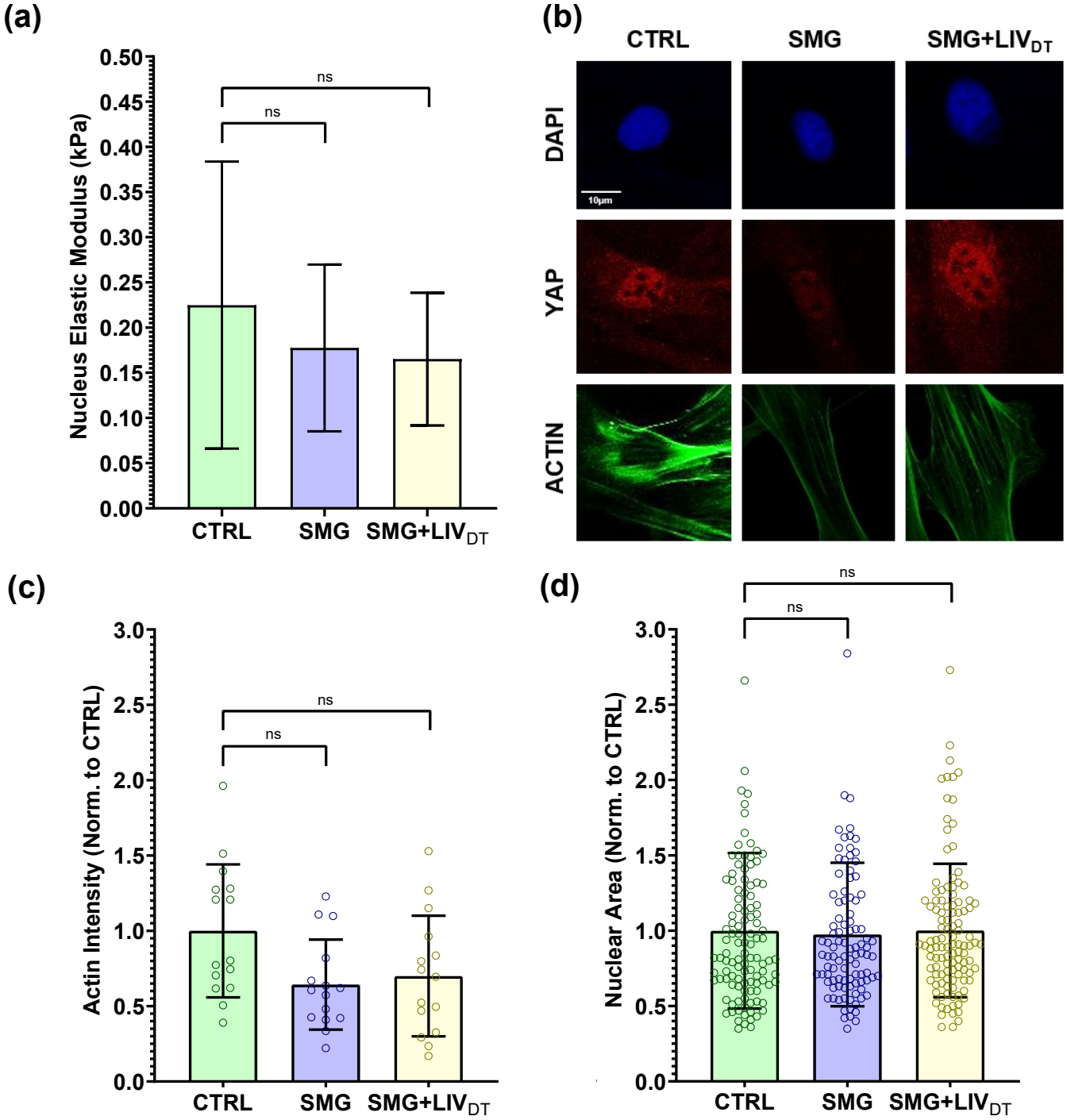


**Figure 7. MSC stiffness and structure remain intact under SMG and SMG+LIV$_{DT}$ treatments.** MSCs were subjected to SMG and parallel SMG+LIV$_{DT}$ over a 72h period. (a) Compared to CTRL samples, AFM measurement of the elastic moduli of SMG and SMG+LIV$_{DT}$ treated MSCs revealed apparent decreases in elastic modules that were 21% and 27% below control levels, measured differences were not statistically significant. n=10/grp. (b) Quantification of confocal images show that, (c) mean F-actin intensity of SMG and SMG+LIV$_{DT}$ treated MSCs revealed decrease of 36% and 30% below control levels, measured differences were not statistically significant. n=15/grp. (d) No significant effects of either SMG or LIV$_{DT}$ treatment on the average nucleus size were found. n>100/grp. Group comparisons were made via Kruskal-Wallis test followed by Tukey multiple comparison, *p<0.05, **p<0.01, ***p<0.01, ****p<0.0001.

# Supplementary Information

## Low Intensity Vibrations Restore Nuclear YAP Levels and Acute YAP Nuclear Shuttling in Mesenchymal Stem Cells Subjected to Simulated Microgravity

Thompson M[1], Woods K[2], Newberg, J[1], Oxford JT, Uzer G[1†]

[1]Mechanical and Biomedical Engineering, Boise State University
[2]Biomolecular Sciences Graduate Program, Boise State University
**[†] Corresponding Author**

**Funding support:**
NASA ISGC NNX15AI04H, NIH R01AG059923, and 5P2CHD086843-03, P20GM109095, P20GM103408 and NSF 1929188.

**Figure S1.**

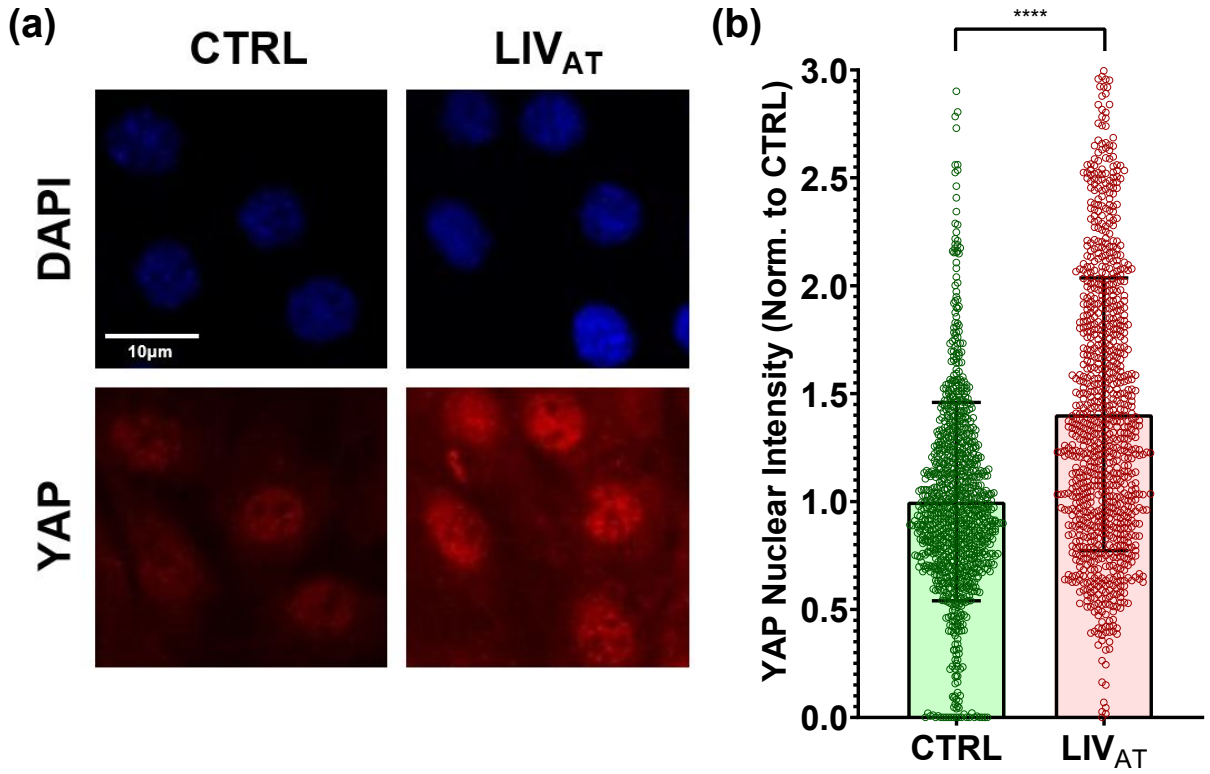


**Figure S1. LIV$_{AT}$ treatment increases nuclear YAP in C2C12 cells.** (a) C2C12 cells were subjected to LIV$_{AT}$ and stained with DAPI (blue) and YAP (red). Confocal images displayed increased nuclear YAP levels following LIV$_{AT}$ treatment. (b) Quantitative analysis of confocal images showed a 40% increase of nuclear YAP in LIV$_{AT}$ samples compared to controls. n>900/grp, group comparison was made using a Mann-Whitney U-test, *p<0.05, **p<0.01, ***p<0.01, ****p<0.0001.

**Figure S2.**

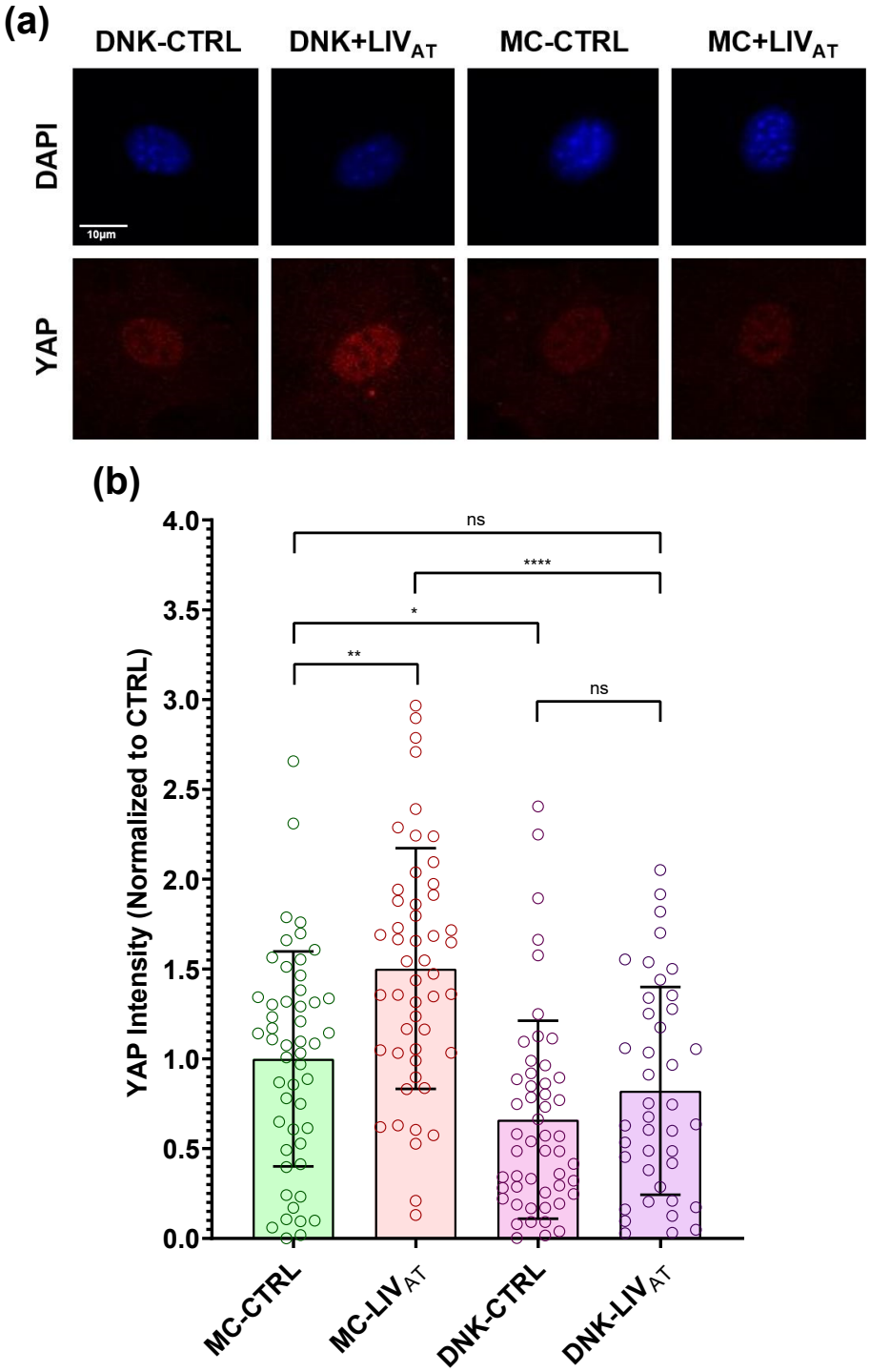


**Figure S2. LINC complex disruption decreases nuclear YAP levels and reduces LIV$_{AT}$-induced YAP nuclear entry.** (a) Plasmids harboring either a dominant negative KASH domain of Nesprin (DNK) to disable LINC complex function or empty mCherry control (MC) were overexpressed in MSCs. Following puromycin selection, MC or DNK expressing MSCs were subjected to LIV$_{AT}$ and stained against DAPI (blue) and YAP (red). (b) Quantitative analysis of confocal images revealed a 49% increase of nuclear YAP following LIV$_{AT}$ in MC expressing control MSCs. Basal YAP levels of the DNK-CTRL group were 34% lower compared to MC-CTRL and LIV$_{AT}$ treatment failed to significantly increase nuclear YAP over DNK-CTRL (18%, NS). n>30/grp, group comparisons were made via Kruskal-Wallis test followed by Tukey multiple comparison, *p<0.05, **p<0.01, ***p<0.01, ****p<0.0001.

**Figure S3.**

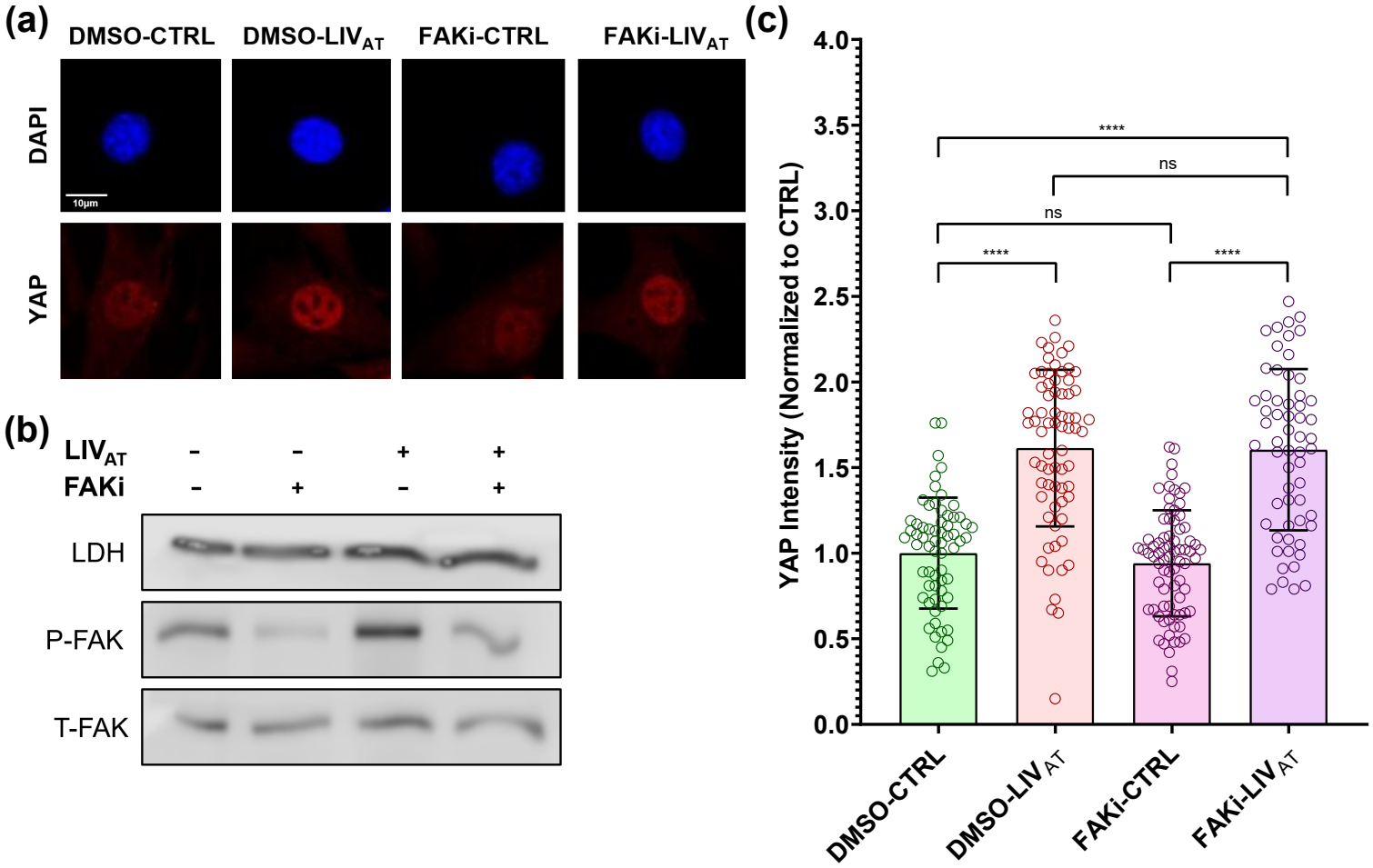


**Figure S3. Blocking FAK phosphorylation at Tyr 397 does not limit LIV$_{AT}$ induced YAP nuclear entry.** Dimethyl sulphoxide (DMSO) or Tyr 397 specific FAK inhibitor (FAKi) PF573228 (3µM) was added to MSCs in culture medium for 1h prior to LIV$_{AT}$ or control treatments. (a) Confocal images of YAP showed more intense nuclear YAP staining of LIV$_{AT}$ treated MSCs but no apparent effect of FAKi when compared to DMSO (b) FAKi application 1hr prior to LIV$_{AT}$ treatment inhibited the LIV$_{AT}$ induced FAK phosphorylation at Tyr 397 and decreased the basal levels (c) Quantitative analysis of confocal images revealed a 61% increase of nuclear YAP in both the DMSO-LIV group and a 60% increase in the FAKi-LIV$_{AT}$ group compared to the DMSO-CTRL group. Differences between the DMSO-CTRL and FAKi-CTRL groups and between the DMSO-LIV and FAKi-LIV$_{AT}$ groups were not significant. n>50/grp. Group comparisons were made via Kruskal-Wallis test followed by Tukey multiple comparison, *$p<0.05$, **$p<0.01$, ***$p<0.01$, ****$p<0.0001$.

**Figure S4.**

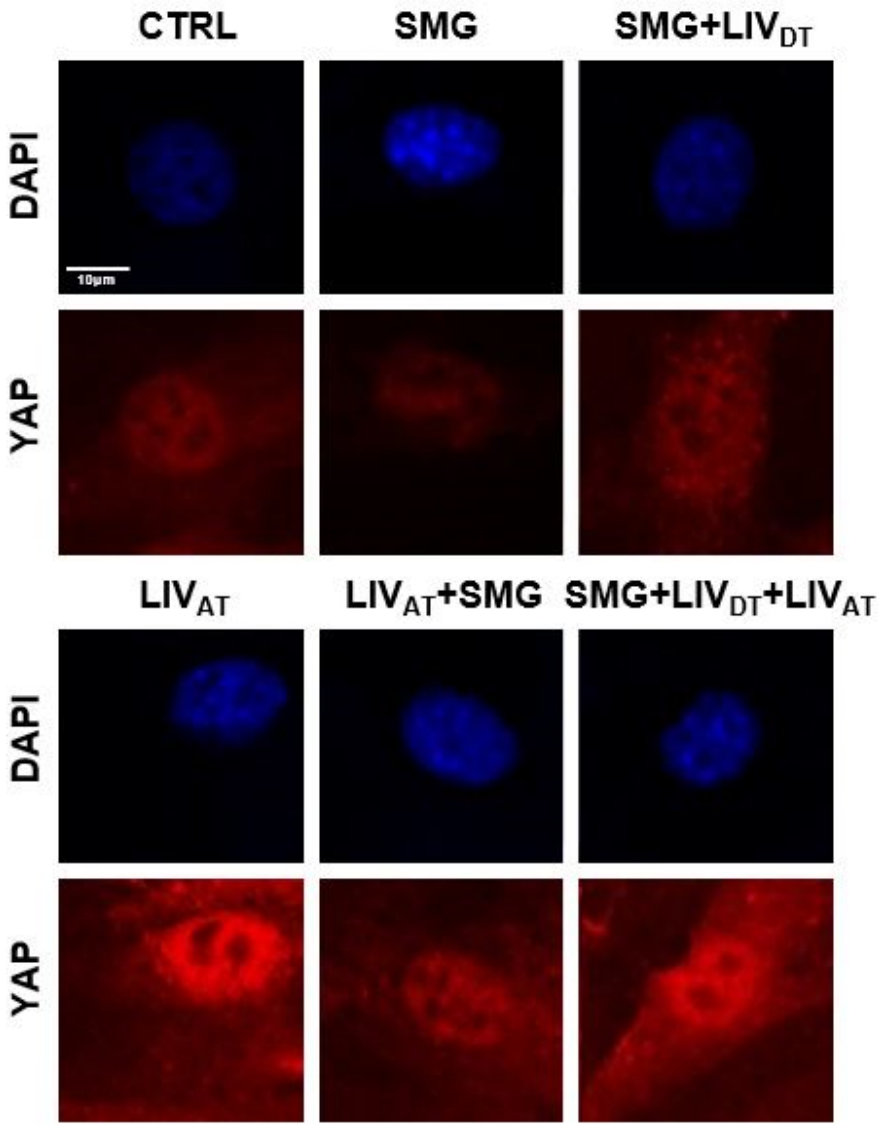


**Figure S4.** Confocal images for SMG/LIV$_{DT}$/LIV$_{AT}$ treatments in Figure 4.

**Figure S5.**

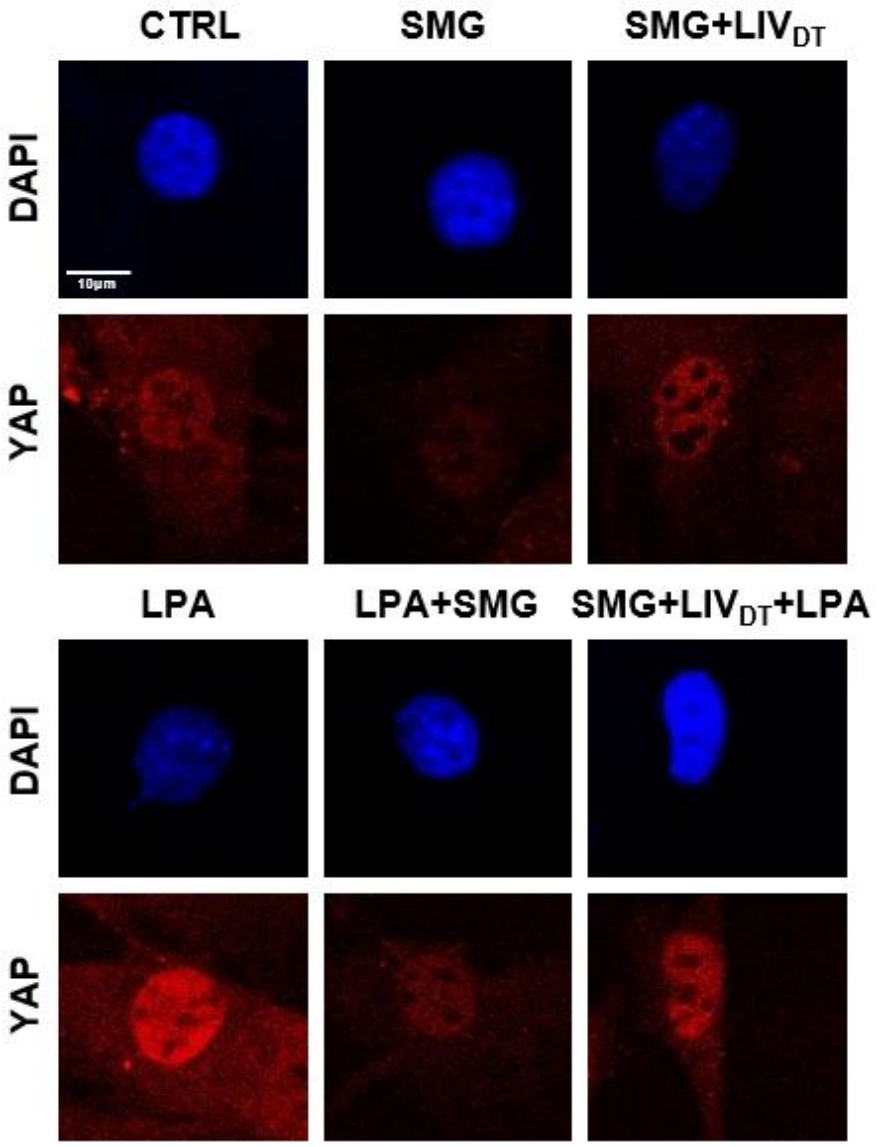


**Figure S5.** Confocal images for SMG/LIV$_{DT}$/LPA treatment in Figure 6.

**Table S1:** Cell culture and pharmacological reagents and their final concentrations.

| Cell culture and pharmacological reagents | | Final Concentration |
|---|---|---|
| IMDM | GIBCO | - |
| DMEM | Caisson Laboratories | - |
| FCS | Atlanta Biologicals | 10% v/v |
| Penicillin/streptomycin | GIBCO | 1% v/v |

**Table S2:** Antibodies used and their final concentrations for western blots.

| Antibodies | | Final Concentration |
|---|---|---|
| p-FAK Tyr397 (3283) | Cell Signaling Technology | 1/1000 |
| FAK (sc-558) | Santa Cruz Biotechnology | 1/500 |
| LDHA (2012S) | Cell Signaling Technology | 1/1000 |

**Table S3:** Immunostaining antibodies and reagents and their final concentrations.

| Immunostaining antibodies and reagents | | Final Concentration |
|---|---|---|
| DAPI (H-1500-10) | Vector Laboratories | 1 µg/mL |
| Alexa Fluor 488 Phalloidin | Life Technologies | 0.1µM |
| YAP (14074S) | Cell Signaling Technology | 1/100 |

# Figure S6

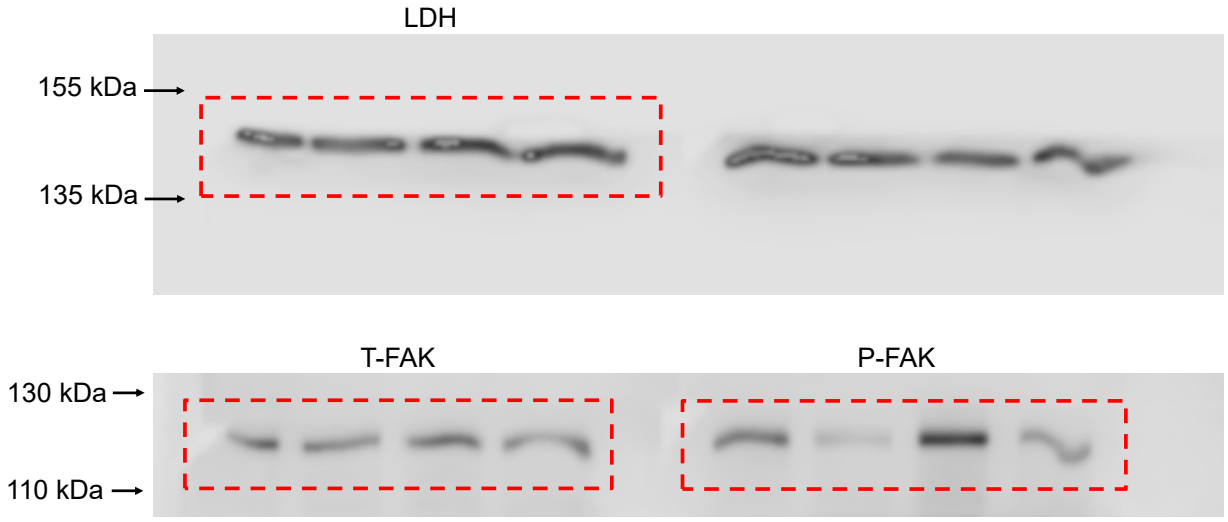


**Figure S6.** Unprocessed blots used in Figure S3 as obtained by LiCor C-DiGit blot scanner.